catalysts

MDPI

Review

Application of EPR Spectroscopy in TiO_2 and Nb_2O_5 Photocatalysis

Osama Al-Madanat [1,2,*], Barbara Nascimento Nunes [1,3], Yamen AlSalka [4], Amer Hakki [5], Mariano Curti [6], Antonio Otavio T. Patrocinio [3] and Detlef W. Bahnemann [1,7,8,*]

1 Institut für Technische Chemie, Leibniz Universität Hannover, Callinstr. 3, 30167 Hannover, Germany; nunes@iftc.uni-hannover.de
2 Chemistry Department, Faculty of Science, Mutah University, Mutah, Al-Karak 61710, Jordan
3 Laboratory of Photochemistry and Materials Science, Institute of Chemistry, Federal University of Uberlandia, Uberlandia 38400-902, Brazil; otaviopatrocinio@ufu.br
4 Institute für Nanophotonik Göttingen e.V., Hans-Adolf-Krebs-Weg 1, 37077 Göttingen, Germany; yamen.alsalka@ifnano.de
5 Center for Industrial Process Technology, Department of Chemical Engineering, KU Leuven, Agoralaan Building B, 3590 Diepenbeek, Belgium; amer.hakki@kuleuven.be
6 Institute of Chemical Research of Catalonia (ICIQ), The Barcelona Institute of Science and Technology (BIST), Av. Països Catalans, 16, 43007 Tarragona, Spain; mcurti@iciq.es
7 Laboratorium für Nano- und Quantenengineering, Leibniz Universität Hannover, Schneiderberg 39, 30167 Hannover, Germany
8 Laboratory "Photoactive Nanocomposite Materials", Saint-Petersburg State University, Ulyanovskaya Str. 1, Peterhof, 198504 Saint-Petersburg, Russia
* Correspondence: al-madanat@iftc.uni-hannover.de (O.A.-M.); bahnemann@iftc.uni-hannover.de (D.W.B.)

Abstract: The interaction of light with semiconducting materials becomes the center of a wide range of technologies, such as photocatalysis. This technology has recently attracted increasing attention due to its prospective uses in green energy and environmental remediation. The characterization of the electronic structure of the semiconductors is essential to a deep understanding of the photocatalytic process since they influence and govern the photocatalytic activity by the formation of reactive radical species. Electron paramagnetic resonance (EPR) spectroscopy is a unique analytical tool that can be employed to monitor the photoinduced phenomena occurring in the solid and liquid phases and provides precise insights into the dynamic and reactivity of the photocatalyst under different experimental conditions. This review focus on the application of EPR in the observation of paramagnetic centers formed upon irradiation of titanium dioxide and niobium oxide photocatalysts. TiO_2 and Nb_2O_5 are very well-known semiconductors that have been widely used for photocatalytic applications. A large number of experimental results on both materials offer a reliable platform to illustrate the contribution of the EPR studies on heterogeneous photocatalysis, particularly in monitoring the photogenerated charge carriers, trap states, and surface charge transfer steps. A detailed overview of EPR-spin trapping techniques in mechanistic studies to follow the nature of the photogenerated species in suspension during the photocatalytic process is presented. The role of the electron donors or the electron acceptors and their effect on the photocatalytic process in the solid or the liquid phase are highlighted.

Keywords: EPR; TiO_2; Nb_2O_5; spin trapping; mechanistic studies

Citation: Al-Madanat, O.; Nunes, B.N.; AlSalka, Y.; Hakki, A.; Curti, M.; Patrocinio, A.O.T.; Bahnemann, D.W. Application of EPR Spectroscopy in TiO_2 and Nb_2O_5 Photocatalysis. *Catalysts* **2021**, *11*, 1514. https://doi.org/10.3390/catal11121514

Academic Editor: Andrea Folli

Received: 1 November 2021
Accepted: 29 November 2021
Published: 13 December 2021

1. Introduction

Heterogenous photocatalytic processes, although attractive for solar energy conversion and environmental remediation, are extremely complex [1–5]. Photon absorption, exciton separation, carrier diffusion, carrier transport, catalytic efficiency, and mass transfer all play major roles [6,7] and can make (or break) the efficiency of the process. Powerful techniques to analyze every step in detail are thus of fundamental importance to overcome bottlenecks

and improve efficiency. Electron paramagnetic resonance (EPR) spectroscopy, also known as electron spin resonance (ESR), differentiates itself from other techniques by providing exceptional sensitivity and specificity towards species with unpaired electrons. Species that can be monitored and characterized by EPR include organic and inorganic radicals, crystal defects (e.g., vacancies or interstitials), dopant atoms, and both free and trapped charger carriers. Photocatalytic reactions (which are radical in nature, see below) and materials are thus very amenable to their study by EPR.

In this short review, we aim to briefly provide the fundamentals of EPR, together with selected examples of its application on well-known photocatalysts, TiO_2 and N_2O_5. We refer the reader interested to have an in-depth view on EPR to the excellent textbooks of Weil and Bolton [8] and Brustolon and Giamello (editors) [9]. Earlier reviews on EPR applied to heterogeneous photocatalysis are also strongly recommended [10–12].

This article is structured as follows. Sections 1.1–1.5, briefly describe the fundamentals of heterogeneous photocatalysis and the EPR technique, together with some special considerations that must be kept in mind when combining them; some important variations on the basic (continuous wave) EPR spectroscopy; and a comparison with other techniques that could be used in a similar fashion. Sections 2 and 3 reviews applications of EPR centered on the photocatalyst itself, covering bare TiO_2 and Nb_2O_5, and surface-modified TiO_2 and Nb_2O_5 systems. Finally, Section 4 presents an overview of EPR applied on the liquid phase in the presence of TiO_2 and Nb_2O_5 materials to elucidate reaction mechanisms, by means of detecting radicals.

1.1. Basic Mechanism of Heterogeneous Photocatalysis

As with all photochemical processes, heterogeneous photocatalytic reactions are initiated by the absorption of light ("Grotthuss-Draper law"). As represented on Scheme 1, excitation of a semiconducting photocatalyst (most commonly TiO_2) with photons carrying enough energy leads to the promotion of an electron from the valence band to the conduction band (e^-_{CB}), leaving behind a hole in the former (h^+_{VB}), Equation (1):

$$TiO_2 + h\nu \rightarrow TiO_2\left(e^-_{CB} + h^+_{VB}\right) \quad (1)$$

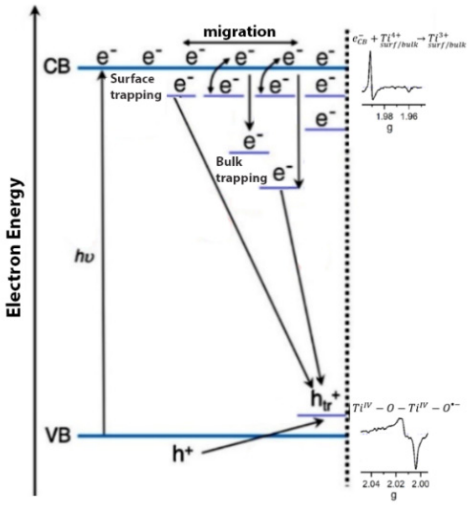

Scheme 1. The possible charge carrier pathways on irradiated TiO_2. Adapted from Reference [13]; Copyright 2019 Elsevier B.V.

In the first instance, both can be thought to be "free", i.e., occupying delocalized states on the respective electronic bands. The fate of most of them is the electron-hole recombination [1], releasing heat to the environment (note: from now on "TiO_2" is omitted for brevity), Equation (2):

$$e^-_{CB} + h^+_{VB} \rightarrow \text{heat} \quad (2)$$

Among the (small) fraction of charge carriers that escape this fate, some are transferred to localized ("trap") states in the semiconductor or its surface, Equations (3) and (4):

$$e^-_{CB} \rightarrow e^-_{Trap} \quad (3)$$

$$h^+_{VB} \rightarrow h^+_{Trap} \quad (4)$$

The exact nature of trapped charge carriers has been the subject of much controversy. However, to a first approximation, electrons can be considered to be trapped at Ti(IV) centers, that could be located either at the surface or bulk of the material (Scheme 1), Equation (5):

$$e^-_{CB} + Ti^{4+}_{surf/bulk} \rightarrow Ti^{3+}_{surf/bulk} \equiv e^-_{Trap} \quad (5)$$

The situation for holes is less clear; regardless, holes are usually considered to be trapped at oxygen atoms on the surface (formally, oxide ions), Equation (6):

$$h^+_{VB} + O^{2-}_{surf} + H^+ \rightarrow HO^{\bullet}_{surf} \equiv h^+_{Trap} \quad (6)$$

Depending on the energy difference to the bands, trap states are normally classified as "deep" or "shallow" [1]. Deeply trapped charge carriers are irreversibly trapped, and less reactive as well, due to the energy dissipation incurred upon trapping. On the other hand, shallowly trapped charge carriers are very close in energy to the valence or conduction band edges, and thus can be excited back just by thermal energy, thus retaining their reactivity [14].

Alternatively, charge carriers (free or shallowly trapped) can be transferred to suitable electron donors (D) and acceptors (A), adsorbed on the semiconductor, Equations (7) and (8):

$$e^-_{CB/Trap} + A \rightarrow A^{\bullet -} \quad (7)$$

$$h^+_{VB/Trap} + D \rightarrow D^{\bullet +} \quad (8)$$

The oxidized and reduced donor and acceptor ($D^{\bullet +}$ and $A^{\bullet -}$, respectively), being radical species, commonly react further via either dark or light-induced reactions to give the final products of the photocatalytic reaction. Common examples are dioxygen as electron acceptor (initially reduced to $O_2^{\bullet -}$) [15] and organic molecules as electron donors (e.g., methanol is initially oxidized to $CH_2OH^{\bullet}$, acetate and oxalic acid) [16,17]. Some authors also consider that holes can be transferred to water to form $OH^{\bullet}$ radicals, although this idea has been repeatedly challenged [18].

1.2. Brief Fundamentals of EPR Spectroscopy

The EPR technique is based on the Zeeman effect, that is, the splitting of electronic energy levels by a magnetic field B_0. For the simple case of a free electron, its spin quantum number is $s = \frac{1}{2}$, with quantized magnetic components $m_s = +\frac{1}{2}$ or $m_s = -\frac{1}{2}$. Its magnetic moment can thus be aligned either parallel or antiparallel (respectively) to the magnetic field (Scheme 2), resulting in different energies, Equation (9):

$$E = m_s g \mu_B B_0 \quad (9)$$

where g is the so-called g-factor (for a free electron, $g = g_e = 2.0023$), and μ_B is the Bohr magneton (9.274×10^{-24} J T^{-1} in SI units). In the absence of a magnetic field ($B_0 = 0$) both magnetic components obviously yield the same energy; while in its presence, the difference in energy (EPR resonance condition) is given by Equation (10):

$$\Delta E = g \mu_B B_0 \quad (10)$$

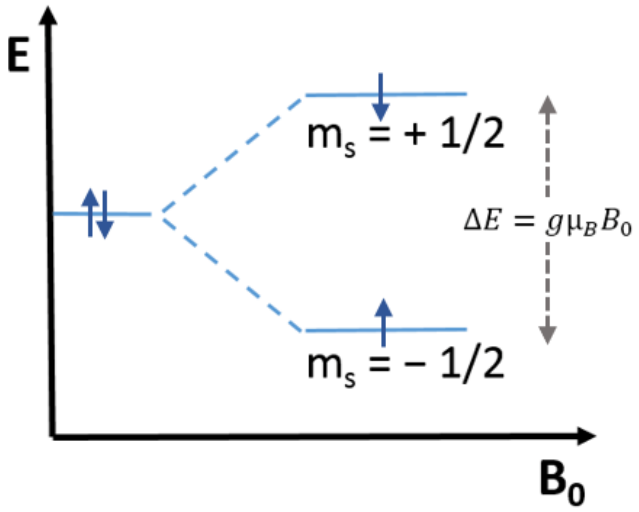

Scheme 2. Schematic representation of the splitting of electronic energy levels by effect of magnetic field B_0.

Importantly, for a bound electron, its g-factor is sensitive to the nature of the paramagnetic center (more specifically, to the atomic or molecular orbital containing the electron). For instance, organic radicals usually exhibit a g factor between 2.002 and 2.006; Cu^{2+} species, between 2.0 and 2.4; and low spin Fe^{3+}, between 1.4 and 3.1.

The different g-factors arise through spin-orbit coupling, which is an anisotropic interaction (related to orbital motion). In consequence, the g-factor is in reality a second-rank tensor (a 3 × 3 matrix), that can be diagonalized to reduce it to three components along the principal axes, Equation (11):

$$[g] = \begin{pmatrix} g_{xx} & g_{xy} & g_{xz} \\ g_{yx} & g_{yy} & g_{yz} \\ g_{zx} & g_{zy} & g_{zz} \end{pmatrix} = \begin{pmatrix} g_x & 0 & 0 \\ 0 & g_y & 0 \\ 0 & 0 & g_z \end{pmatrix} \quad (11)$$

Considering this, the resonance condition becomes (Equation (12)):

$$\Delta E = \mu_B \left(g_x B_x + g_y B_y + g_z B_z \right) \quad (12)$$

where B_x, B_y, and B_z are the components of the magnetic field along the principal axes. This is relevant, for instance, in the case of rhombic crystal structures (e.g., brookite TiO_2). If there is axial symmetry (as in anatase and rutile TiO_2), two of the components are identical: $g_x = g_y$; the two different components are usually labeled as $g_x = g_y = g_\Delta$ and $g_z = g_{||}$. In fluid media, all orientations are averaged, resulting in a single, isotropic (averaged) g value, Equation (13):

$$g_{iso} = \frac{1}{3}\left(g_x + g_y + g_z \right) \quad (13)$$

In addition to the Zeeman interaction, the interaction between the magnetic moment of the electron with the magnetic dipole moment of the nuclei of the paramagnetic center and surrounding atoms (I) must also be considered. Usually smaller in magnitude than the Zeeman interaction, the incorporation of this so-called "hyperfine interaction" affects the resonance condition as follows (Equation (14)):

$$\Delta E = g\mu_B B_0 + \sum_i S A_i I_i \quad (14)$$

where the index i runs overall interacting nuclei, A_i is the hyperfine matrix corresponding to nucleus i, and $S = \frac{1}{2}$ for a radical. Generally, the hyperfine interaction has isotropic and anisotropic components, resulting in a matrix that describes this effect. Importantly,

as a consequence of the hyperfine interaction, each EPR line is split into several lines. In the simple case of a single nucleus with nuclear spin I, the spectrum will consist of $2I + 1$ lines; more generally, for k nuclei, there will be $\prod 2I_k + 1$ lines. Additional types of interactions, such as the superhyperfine splitting, are described elsewhere and are generally less important [9].

EPR spectroscopy experiments can be performed at different resonant frequencies. The most common one is the so-called X-band: by applying a magnetic field B_0 of ~3480 G, the resonance frequency v is ca. 9.75 GHz (the exact values depend on the g-factor), i.e., in the microwave region, Equation (15):

$$\Delta E = hv = g\mu_B B_0 \quad (15)$$

For practical reasons, typically the microwave frequency is kept fixed, while the magnetic field is varied to sweep the region of interest. In addition, the field is usually modulated; this allows to apply lock-in amplification, improving the sensitivity of the technique. As a result, EPR spectra are normally measured as the first derivative of the absorption spectra. The latter can be easily recovered by integrating the measured signal; double integration yields peak areas, proportional to the number of spins in the sample.

1.3. Special Considerations and Limitations on the Use of EPR

In relation to the photocatalysts materials, the paramagnetic species involved on the photocatalytic processes include the trapped photogenerated carriers, that is, electrons and holes, some inorganic active species on EPR as transition metal ions, or also the species formed on the photocatalyst surface by the redox reactions such as reactive oxygen species, and organic radicals. More detailed information regarding paramagnetic species on heterogeneous photocatalysis and the EPR technique was reviewed by Wang and coauthors [10]. In relation to the radicals formed by the photocatalyst after the redox reactions, although EPR is extremely sensitive, species with unpaired electrons are generally very reactive. Thus, even if a radical of interest is continuously produced (e.g., by continuous irradiation), its steady-state concentration may be too low for it to be detected. An extensively employed workaround is the use of so-called "spin-traps", diamagnetic compounds that readily undergo addition reactions with radicals to produce a new radical species with higher stability (and thus allow their detection). Generally, hyperfine splitting results in a distinctive spectrum for different adducts, allowing their identification.

A commonly used group of compounds are nitrones, which can "trap" a radical $R''^{\bullet}$ as follows, Equation (16):

$$RHC = N^+O^-R' + R''^{\bullet} \rightarrow RR''^{\bullet}HC = NO^{\bullet}R' \quad (16)$$

For instance, DMPO (5,5-Dimethyl-1-Pyrroline-N-Oxide) is commonly employed to trap $OH^{\bullet}$ [19], $CO_2^{-\bullet}$, and the organic radicals [20–23]. It can also be employed to detect the superoxide radical $O_2^{\bullet-}$, although in that case the trapping reaction is hindered by a slow rate, and the formed adduct presents a similar spectrum to that of other peroxyl adducts [24].

The use of low temperature (below 77 K) can also improve detection by decreasing diffusion rates–and thus reactivities. This is particularly important to monitor charge carriers in photocatalysts, where room temperature measurements are commonly impossible due to fast recombination. In fact, Howe and Grätzel were the first to detect the presence of trapped electrons and did so by freezing degassed acidic suspensions of colloidal TiO_2 after room temperature irradiation [25].

In the case of Ti^{3+} species, the situation is worsened by the very short spin-lattice relaxation times that decrease EPR sensitivity towards these species. Remarkably, Grela and coworkers were able to detect Ti^{3+} centers at room temperature by irradiating chloride-containing ethanolic TiO_2 sols [26], although generally speaking this is not feasible with photocatalytic materials, and liquid nitrogen temperatures are mandatory. It is important

to note, however, that the conclusions drawn under such conditions may not be completely transferrable to the photocatalytic process under *operando* conditions.

1.4. Comparison with Other Techniques

Several techniques can monitor photogenerated charge carriers and radical species produced during photocatalytic reactions. The main distinguishing factor of EPR is the fact that it is exclusively and strongly sensitive to species with unpaired electrons. Since closed-shell species are EPR-silent, signal assignment is simplified with respect to more general techniques; in addition, minute amounts (in the order of 10^9 spins) of unpaired species can be readily detected. As described above, trapped charge carriers, and the species produced after electron transfer to (from) acceptors (donors), are radicals, and thus EPR provides an invaluable tool to study photocatalytic processes (Scheme 1). Its main shortcomings are those described in Section 1.3.

A commonly employed alternative technique is transient absorption spectroscopy (TAS) [27]. A clear advantage of TAS over EPR is its very high time resolution, in the order of ns (or even shorter timescales for pump-probe setups), which can provide fundamental information on the processes. However, interpretation is usually very complex: band assignments are hindered by the confounding facts of low spectral resolution, inherent noise in the measurements, broadness of the signals, and most importantly, the low specificity of the technique (i.e., most species show a signal in TAS). An additional problem relative to transient absorption techniques applied to photocatalysis is that spectral characteristics are strongly dependent on particle size [28], crystal phase, and surface conditions, rendering direct comparison of spectra corresponding to differently prepared photocatalysts a difficult task. Finally, the (usually) large number of electron-hole pairs generated per particle upon laser excitation may not adequately reflect the properties of the system under weaker irradiation.

Diffuse reflectance Fourier transform infrared spectroscopy (DRIFTS) has also been employed to monitor free and trapped charge carriers in TiO_2 [29,30]. An important shortcoming of this technique is that both water and organic solvents strongly absorb in the infrared region, practically preventing their use [31]. If the process of interest occurs in the suspension or liquid phase, as is usually the case, the conclusions from DRIFTS studies may not be transferrable. In addition, at least in the case of TiO_2, it is believed that only electrons (i.e., not holes) present a signal in DRIFTS [31].

Another technique that can be used to get insights into photogenerated charge carriers is time-resolved microwave conductivity (TRMC) [32–34]. In this case, an important shortcoming is the fact that only free electrons are detectable by TRMC. On the other hand, it is possible to perform TRMC measurements under conditions relatively similar to those of photocatalytic reactions.

In some cases, a combination of different techniques would provide additional informative results. For example, by combining EPR with IR techniques, it has been demonstrated that free carriers in TiO_2 samples are EPR silent and only trapped species can be detected [35]. The situation in ZnO quantum dots is completely different. In this oxide, free conduction-band electrons can be readily monitored by EPR spectroscopy at room temperature, and its g values correlate with the nanocrystal size [36]. By exploiting this finding, unexpected electron transfer between electron-charged and uncharged capped nanoparticles [37] was recently discovered by Gamelin and coworkers. It is apparent that the ability of monitoring primary carriers in conditions that closely match practical operational situations will provide new insights into nanoscale ET processes, in the near future.

Interestingly, EPR is able to sense the local environment of the trapped species. This possibility has recently been exploited to get some understanding for the enhanced photocatalytic activity of mixed-phase anatase- rutile TiO_2 specimens [38] and to study the effect of shape and size on the paramagnetic species formed upon UV excitation of TiO_2.

1.5. EPR Derivatives

Generally speaking, the spectra in the continuous wave EPR method (*CW EPR*) are recorded by putting a sample into an MW irradiation field of constant frequency ν and sweeping the external magnetic field B_0 until the resonance condition is fulfilled. In *pulse EPR* the spectrum is recorded by exciting a large frequency range simultaneously with a single high-power MW pulse of given frequency ν at a constant magnetic field B_0. Pulse EPR technique is extremely useful for the study of spin-dependent transport processes, and it opens the door of the time-domain realm and in turn to the Fourier transform of the time traces for a frequency-domain characterization. Therefore, pulse EPR is relevant in understanding the photocatalytic behavior of materials such as TiO_2 [1,10,11]. By means of pulse-EPR hyperfine techniques, the problem of the localization of the electron spin density can be tackled. Employing this technique, Chiesa et al. [39] were able to prove the substantial difference, in terms of wavefunction localization between anatase (electrons trapped in regular lattice sites exhibiting delocalized electron density) and rutile (interstitial sites showing localized electron density). With the help of pulse EPR, Dimitrijevic et al. [40] have observed different spin dynamics for different shapes of anatase nano-objects which in turn results in differences in the charge separation efficiencies and electron-hole recombination probabilities.

In addition, a recent innovation in the EPR approach to study trapped electrons and holes there is the use of the ^{17}O isotope. This isotope, bearing a nuclear spin $I = \frac{5}{2}$, when introduced in the oxide, allows the observation of hyperfine interactions that are not visible when oxygen is present in its natural abundance (essentially ^{16}O with zero nuclear spin). This approach, coupled with the highly sensitive pulsed EPR techniques (since the ^{17}O hyperfine couplings are usually very small, they escape detection with classic CW-EPR), which has allowed the description of the coordination sphere of either chemically generated or photogenerated Ti^{3+} centers. Using selective isotopic enrichment, it was possible to discriminate the Ti^{3+} located in the bulk from those located at the surface, for instance, in interstitial centers in TiO_2 rutile [41], in TiO_2 anatase [42], and TiO_2 rutile and brookite polymorphs [43].

2. Titanium Dioxide Photocatalyst

Titanium dioxide (TiO_2) is a solid material used in large-scale practical applications, including photocatalysis. It has been used in many photocatalytic reactions, e.g., the mineralization of water and air pollutants, super hydrophilicity, and solar energy conversion [44]. Titanium dioxide has three polymorphs, i.e., rutile (the thermodynamically stable phase), anatase, and brookite. These polymorphs are built up by distorted octahedral TiO_6 units, in which the oxygen atoms are surrounded by three Ti ions (OTi_3). Although some papers have reported promising activity for the brookite phase, the most investigated polymorphs are rutile and anatase They are differed from each other by their bandgap energy (3 and 3.2 eV for rutile and anatase, respectively), and by the more stable crystal faces (110 and 101 for rutile and anatase, respectively) [1].TiO_2-based photocatalytic processes are induced by an initial excitation through the irradiation by a suitable light source, having an energy equal to or higher than the band-gap energy of the TiO_2 [45].

The irradiation of TiO_2 by a suitable light leads to a charge spatial separation, i.e., the promotion of an electron (e^-) in the conduction band (CB) and the formation of a hole, (h^+) in the valence band (VB). These charge carriers can be then migrated and trapped at the surface of TiO_2, before their transfer to the adsorbed species at the surface [46]. The trapped electrons and trapped holes can also be promoted due to chemical modifications of TiO_2. While anatase has shown better photocatalytic activity than rutile, the mixed-phase Degussa P25 has demonstrated, in some cases, better activity due to the presence of an interface between the anatase and rutile, which improves the spatial separation of the photo-generated charge carriers [47]. Nevertheless, the recombination of charge carriers, the nature and location of the charge traps, and the stability of the trapped charge carriers are important phenomena that affect the overall photocatalytic activity. The

photocatalytic activity of TiO_2 is highly related to its surface properties and, therefore, it is of high importance to investigate TiO_2 from the surface science point of view. Titanium dioxide is considered a reducible metal oxide because it can lose oxygen, forming oxygen vacancies and excess electrons, as can be seen in Equation (17) [48]. The insulating TiO_2 turns into an n-type semiconductor due to oxygen depletion, while the excess electrons are stabilized into the reduced solid and trapped as Ti^{3+} centers. Thus, when excess electrons are photogenerated in TiO_2, they are usually stabilized by Ti cations with the formation of Ti^{3+} ions.

$$O_2^- + 2Ti^{4+} \rightarrow \frac{1}{2}\,O_2 + V_O^{\bullet\bullet} + 2Ti^{4+} + 2e^- \rightarrow \frac{1}{2}\,O_2 + V_O^{\bullet\bullet} + 2Ti^{3+} \quad (17)$$

$V_O^{\bullet\bullet}$ is an empty vacancy in the Kröger–Vink notation.

The generation of Ti^{3+} upon the irradiation of TiO_2 has been detected by Electron Energy Loss Spectroscopy (EELS) [49], stopped-flow spectrophotometry [50], laser-flush photolysis [44], polarized optical spectroscopy [51], photoelectron spectroscopy [52], and Electron Paramagnetic Resonance spectroscopy (EPR) [53]. EPR spectroscopy is considered as a sensitive technique to follow the surface defects and the radical formation at semiconductor surfaces, especially the paramagnetic species and the hyperfine interaction. EPR spectroscopy has been mainly employed to investigate the surface chemistry of polycrystalline TiO_2, i.e., the formation of Ti^{3+} centers under irradiation or other conditions and its reactivity towards different adsorbed species. It is also very useful in clarifying the charge trapping and the surface charge transfer upon irradiating the surface of TiO_2.

2.1. Trapped Electrons and Holes in TiO_2: EPR and g Tensor

TiO_2 has been mainly investigated employing the Continuous Wave-EPR (CW-EPR) technique, which commonly uses X-band microwaves having 9.5 GHz frequency and generates the spectrum of the first derivative of the microwave absorption as a function of the magnetic field (Tesla or Gauss). Upon irradiation, the photogenerated electrons are trapped as Ti^{3+} centers, which have paramagnetic properties ($S = \frac{1}{2}$) having a $3d^1$ configuration. When the metal ion is octahedrally coordinated, as in the case of all TiO_2 polymorphs, the free-ion ground state is split into two subgroups having three t_{2g} and two e_g orbitals separated by the energy term Δ_O. The degeneracy of the t_{2g} and e_g levels owing to a tetragonal (Scheme 3A) or trigonal (Scheme 3B) distortion leads to anisotropic g values [39].

When the distortion compresses the tetragonal (D_{4h}), the d_{xy} orbital is the ground state, however, if the distortion elongates this tetragonal, the ground state is a degenerate d_{xy}, d_{yz} orbital. The g values for a Ti^{3+} in a tetragonally distorted octahedral environment are:

$$g_{II} \approx g_e - (8\lambda/\delta_2) \text{ and } g_I \approx ge - (2\lambda/\delta_1)$$

where λ is the spin-orbit coupling constant for Ti^{3+} (154 cm^{-1}), δ_1 and δ_2 are the energy separation between the d-orbitals (Scheme 3A) [39].

On the other hand, the photoexcitation of TiO_2 photocatalyst produces a paramagnetic center, i.e., O^- ion due to the hosting of the unpaired electron in the 2P orbital of the oxygen atom ($O^{2-} + h^+ \rightarrow O^-$). In this case, the g tensor can be either axial ($g_{II} = g_{zz} \approx g_e$; $g_I = g_e + 2\lambda/\Delta E$) or rhombic ($g_{zz} \approx g_e$; $g_{xx} = g_e + 2\lambda/\Delta E_1$; $g_{yy} = g_e + 2\lambda/\Delta E_2$) depending on the symmetry of the environment (Scheme 4) [39].

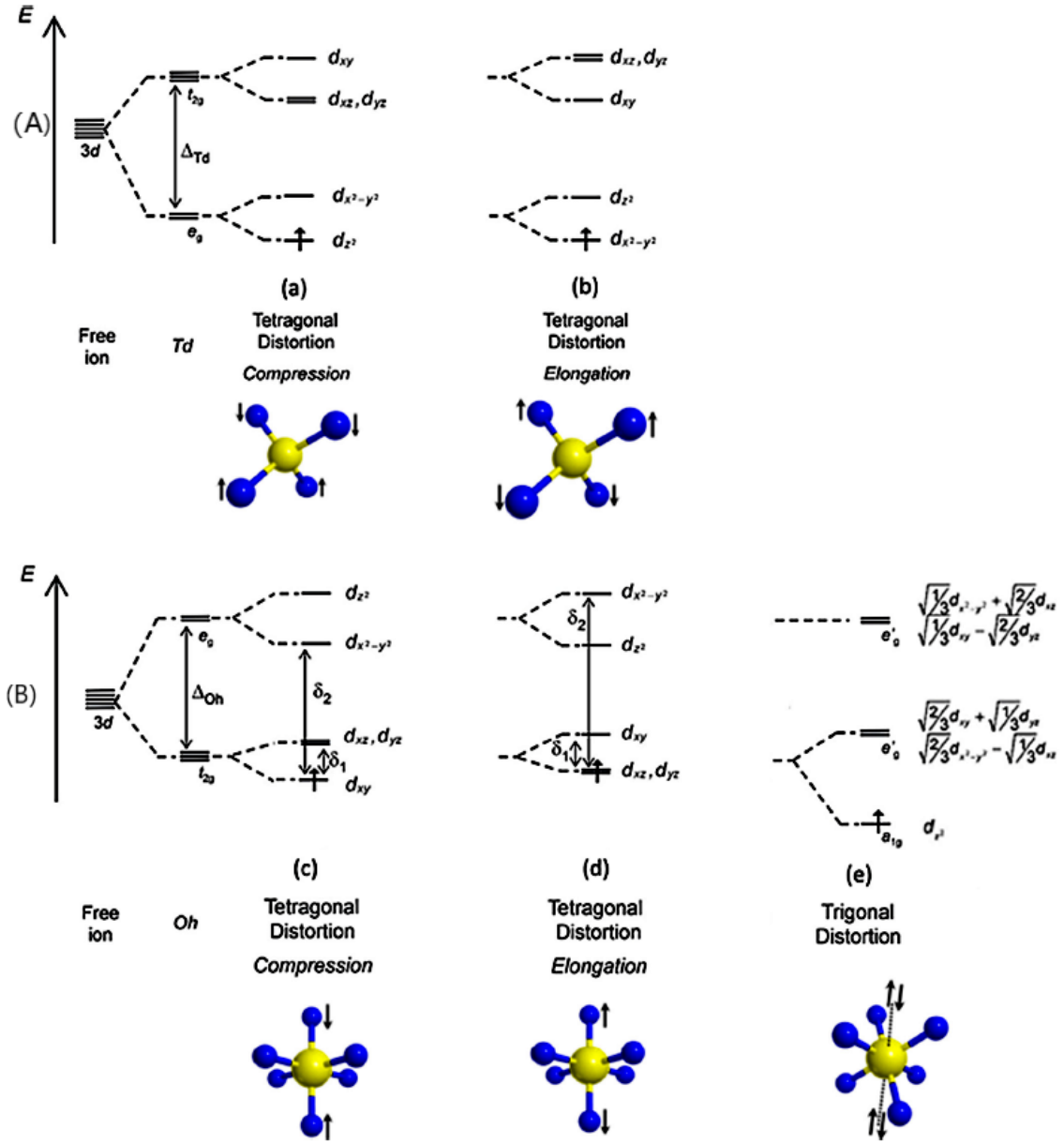

Scheme 3. The level of the d-orbitals of Ti^{3+}: (**A**) tetragonal and (**B**) trigonal distorted octahedral crystal field. Reprinted with permission [54].

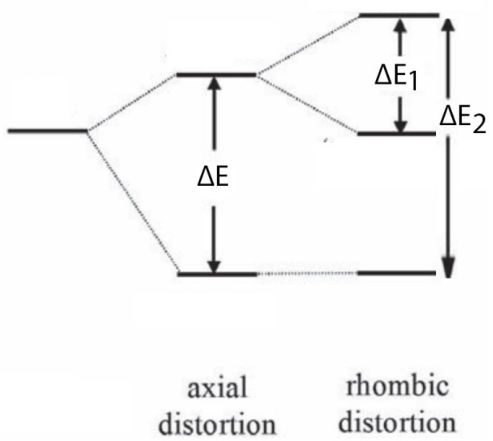

Scheme 4. Energy levels of O ions in axial and rhombic symmetry.

2.2. Charge Trapping Centers in Photoexcited TiO_2

In-situ EPR investigations have been widely done especially for anatase, rutile, and mixed-phase P25 TiO_2 photocatalysts under irradiation. These investigations were performed either for TiO_2 suspensions in aqueous phases, or for dehydrated TiO_2 powders at the solid-gas interfaces. In the former case, the presence of hydroxyl ions and water molecules on the surface of TiO_2 stabilizes longer the charge carriers.

In their premier work to study the paramagnetic species on semiconducting photocatalysts, Howe and Grätzel [25] have reported an EPR observation of trapped electrons in irradiated colloidal TiO_2. Although a blue coloration of TiO_2 suspension appeared upon the irradiation of degassed acidic solution of colloidal TiO_2 in the presence of PVA (polyvinyl alcohol), no EPR signals were detected at room temperature. However, the authors were able to detect such signals at 77 K after the irradiation at room temperature. They showed that the collected spectra consisted mainly of two overlapping signals: (i) a broad signal at g = 1.92, and (ii) a smaller and narrower feature at g = 1.988, which was more pronounced in lower concentrated solutions as presented in Figure 1b. In alkaline solution, the broad signal at g = 1.93 was less intense and the signal at g = 1.988 was better resolved as the perpendicular component of an axially symmetric signal with the corresponding parallel component of g = 1.957 (Figure 1c).

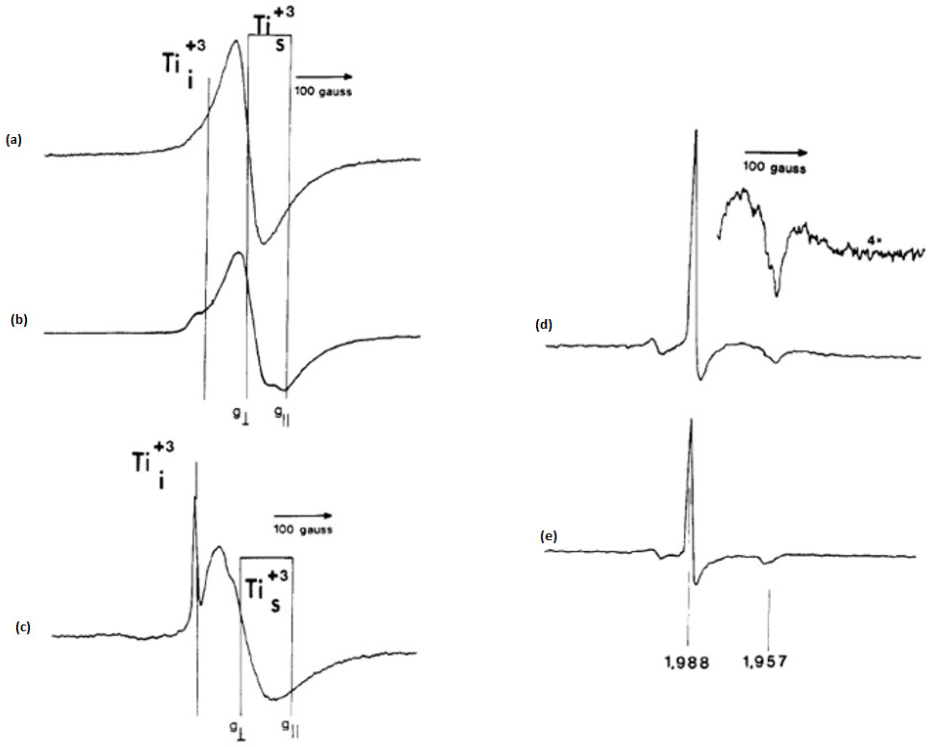

Figure 1. EPR spectra of colloidal TiO_2 solutions at pH 2.2 containing PVA after irradiation at room temperature (recorded at 77 K): (**a**) 13 g of Ti0 dm^{-3}; (**b**) 5.3 g of TiO_2 dm^{-3}; EPR spectra of colloidal TiO_2 solutions at pH 10.6 containing PVA after irradiation at room temperature recorded at 77 K (**c**); EPR spectra of colloidal TiO_2 solutions irradiated at 77 K: (**d**) pH 2.2, 5.5 g dm^{-3}, containing PVA; (**e**) the same solution without PVA. Adapted from [25]. Copyright 1985 American Chemical Society.

However, the authors noticed that a narrow axial signal was most prominent when the irradiation and the detection were carried out at 77K as can be seen in Figure 1d. They clarified that in all signals the g values below 2 were due to the formation of Ti^{3+} species and the insensitivity of the narrow line to changes in pH reveals that Ti^{3+} species are located in the interior of colloid particles. They commented also that the values of the g-tensor components for the colloid Ti^{3+} signals are significantly lower than those for Ti^{3+} in powdered TiO_2. The authors have also found that the presence of a hole scavenger induced

many electrons to be trapped at surface Ti^{4+} sites, generating Ti^{3+} species with distorted octahedral that responsible for the blue color and the broad EPR signals. Using a hole scavenger in the absence of oxygen, both surface and bulk trapped electrons were stable at room temperature. The irradiation of the suspension in presence of a hole scavenger at 77 K produced faster bulk trapped electrons than those trapped at the surface Figure 1d,e. The authors suggested that the origin of the blue color in irradiated colloids was not due to electrons trapped at oxide vacancies because no EPR signals at g = 2.0 were observed. Hence, they distinguished the surface Ti^{3+} species from the interstitial Ti^{3+} species and showed that increasing the acidity and temperature of the suspension induces the trapping of electrons in surface sites.

In another publication, Howe and Grätzel [55] did an EPR study of hydrated anatase, in which a high-vacuum sample cell was immersed in the liquid helium (4.2 K) or in the liquid nitrogen (77 K) and irradiated with a 450-W xenon lamp. Upon the irradiation at 4.2 K, hydrated anatase produced an EPR spectrum that consisted of two signals as shown in Figure 2a: a low-field slightly nonaxial signal (signal B) and a high-field axial signal (signal A), which was disappeared in the presence of traces of residual oxygen. These signals were stable with time, however, they decayed rapidly when the lamp was turned off. On the other hand at 77 K, an order of magnitude less intense identical signals have appeared. In this case, signal B was only produced upon the irradiation in the presence of O_2 and was stable even in the dark (Figure 2b). While the authors attributed the high-field signal A (g_1 = 1.990, g_2 = 1.990, g_3 = 1.960) to interstitial Ti^{3+} cations, they assigned the low-field signal B (g_1 = 2.016, g_2 = 2.012, g_3 = 2.002) to the trapping of positive holes at lattice oxide ions. The trapped holes could be located in the subsurface layer as $Ti^{4+}O^{-}Ti^{4+}OH$ since signal B was not broadened by the presence of O_2. The authors considered different possible pathways for the generation of these paramagnetic species. Upon the irradiation at 4.2 K, most of the charge carriers are trapped, i.e., electrons as Ti^{3+} and holes at subsurface oxide ions, which are then quickly recombined each other after turning off the lamp, decaying the EPR signals. The adsorbed oxygen prevents recombination and stabilizes the trapped holes by scavenging the trapped electrons through a multielectron process. They concluded also that the existence of hydroxyl radicals on the surface appears to be transient and they were apparently not primary products of hole trapping.

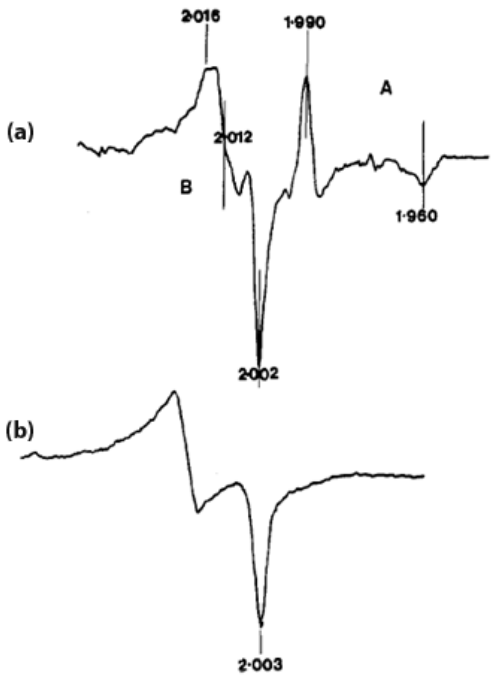

Figure 2. EPR spectra of (**a**) hydrated anatase irradiated in vacuo at 4.2 K; (**b**) irradiated in 30 mbar of O_2 at 77 K. Adapted with permission from [55]. Copyright 1987 American Chemical Society.

Micic et al. [56] investigated the trapped holes on colloidal TiO_2 by EPR spectroscopy, in which they assigned the signals at g < 2 (see Figure 3a) to the capture of electrons on by Ti^{4+} ions. They showed a broad asymmetric EPR signal at g = 1.928 of Ti^{3+} species at surface sites, in addition to a narrower EPR signal at g = 1.987 of trapped electrons at interior sites since it was not affected by the presence of electron scavengers. The authors clarified that as the photogenerated electrons can be located on Ti^{4+}, in the bulk lattice as $(Ti^{3+})_{latt}$, at the surface as (Ti^{3+})surf, and in the conduction band $[e^-_{CB}]$. On the other hand, the signals with g = 2.007, g = 2.014, and the shoulder at about g = 2.020–2.028 were assigned to hole centers on the surface or subsurface layers because their intensities had been suppressed in the presence of polyvinyl alcohol or KI as hole scavengers. They explained that the surface of anatase TiO_2 is covered with hydroxide ions or water molecules with an average number of 5–15 OH^- groups per nm^2. Part of these hydroxide ions that are located on the (110) surface of TiO_2 can therefore trap the photogenerated holes. Such hydroxide ions are present as acidic Ti^{4+}-O(H)-Ti^{4+} and basic Ti^{4+}-OH groups. Because the latter has a higher electron density, it is expected to be the primary hole trapping site. They showed also that the relative intensities of the EPR signals at g = 2.014 and 2.007 changed with pH. This was associated with the ionic form dominated by Ti^{4+}-OH groups (Equations (18) and (19)). The authors investigated as well the EPR signals of anatase and rutile TiO_2 powders suspended in water as presented in Figure 3b,c. Same signals were obtained for anatase as for the colloidal TiO_2 but with lower intensities. The authors attributed that to the smaller surface area for suspended anatase TiO_2 powder. Nevertheless, a very weak signal was noticed for rutile powder that was similar to one of those found in anatase particles. The authors ruled out the OH radicals to be the species produced by hole trapping. They suggested instead an oxygen-centered radical, which can most probably be a hole trap on the basic OH-group having an energy level below the valance band of TiO_2 as illustrated in Equation (20). This was explained by the fact that such a group has a higher electron density. Such trapped holes can react through a direct transfer mechanism with chemical substrates adsorbed on the surface as in the case of methanol in the aqueous colloidal TiO_2 solution.

$$Ti^{IV} - O - Ti^{IV} - OH + H^+ \leftrightarrow Ti^{IV} - O - Ti^{IV} - OH_2^+ \quad (18)$$

$$Ti^{IV} - O - Ti^{IV} - OH \leftrightarrow Ti^{IV} - O - Ti^{IV} - O^- + H^+ \quad (19)$$

$$H^+ + Ti^{IV} - O - Ti^{IV} - OH \rightarrow Ti^{IV} - O - Ti^{IV} - O^{\bullet -} + H^+ \quad (20)$$

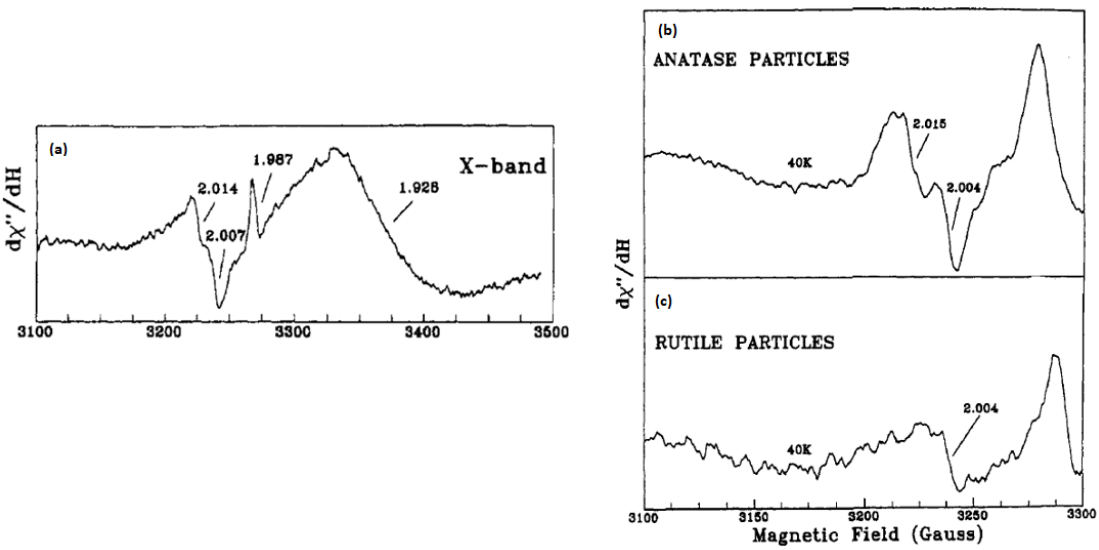

Figure 3. EPR spectrum of degassed aqueous colloidal $Ti0_2$, pH 3, irradiated at 77 K with a 308 nm excimer laser (**a**); EPR spectra of $Ti0_2$ powder suspended in degassed water irradiated at 77 K (**b**) anatase, recorded at 40 K, (**c**) rutile, recorded at 40 K. Adapted with permission from [56]. Copyright 1993 American Chemical Society.

In another work, Micic et al. [57] presented an EPR study for the hole transfer from irradiated TiO_2 colloids to methanol in an aqueous solution. Upon the excitation of degassed solutions of alkoxide TiO_2 colloids at different temperatures, they noticed three different signals around g = 2. At high laser pulse intensities, a quartet EPR signal (1:3:3:1) and a doublet signal with a 130-G separation appeared at 4.2 K as shown in Figure 4a and were attributed to the methyl (CH_3) and formyl (CHO) radicals (Equations (21)–(24)), respectively. However, at 60 K (Figure 4b), the EPR signal of the methyl radical disappeared, while the other signal can be related to the methanol radical [$CH_3O(H)$]. The authors suggested possible pathways for radical formation as per, Equations (25) and (26). On the other hand, the EPR signal for trapped holes on hydrous TiO_2 colloids showed resonances at g = 2.014 and g = 2.007 of $O^{\bullet -}$ radical with an additional signal at g = 1.989 of electron trapping in the bulk lattice. In this case, hydroxide ions on the surface can be the trap centers for photogenerated holes. Then they obtained at 1.9 K EPR signals of methanol radical (20-G splitting around g = 2) and Ti^{3+} centers at (g = 1.980, g = 1.960, and g = 1.942) due to the addition of methanol to the aqueous TiO_2 solution as can be seen in Figure 5, suggesting that $^{\bullet}CH_2OH$ radicals are the first hole trapping sites.

$$TiO_2 \xrightarrow{h\nu} n\left(e^- + H^+\right) TiO_2 \tag{21}$$

$$e^- + Ti^{IV} - O - Ti^{IV} - OCH_3 \leftrightarrow Ti^{IV} - O - Ti^{IV} - O^- + CH_3^{\bullet} \tag{22}$$

$$h^+ + Ti^{IV} - O - Ti^{IV} - OCH_3 \leftrightarrow Ti^{IV} - O - Ti^{IV} - O^{\bullet}CH_2 + H^+ \tag{23}$$

$$Ti^{IV} - O - Ti^{IV} - O^{\bullet}CH_2 + H_2O \xrightarrow{h\nu} {}^{\bullet}CHO + H_2 + Ti^{IV} - O - Ti^{IV} - OH \tag{24}$$

$$h^+ + Ti^{IV} - O - Ti^{IV} - OH \rightarrow Ti^{IV} - O - Ti^{IV} - O^{\bullet} + H^+ \tag{25}$$

$$h^+(TiO_2) + CH_3OH \rightarrow {}^{\bullet}CH_2OH + TiO_2 + H^+ \tag{26}$$

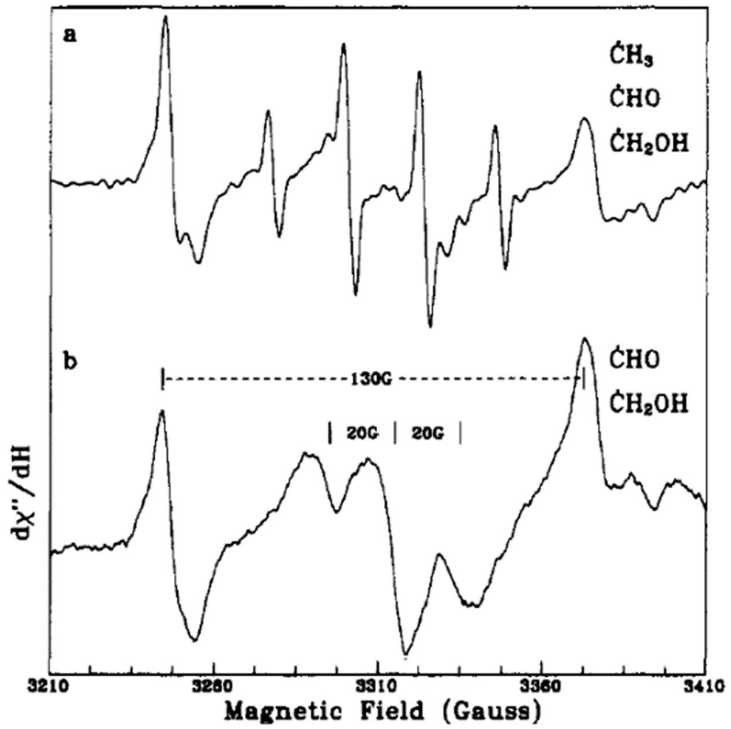

Figure 4. EPR spectra of degassed colloidal $Ti0_2$ at pH 8 prepared in methanolic solution, evaporated, and then dissolved in water, recorded immediately after laser irradiation at 4.2 K with laser intensity 120 mJ/pulse (**a**); laser intensity 120 mJ/pulse, recorded at 60 K (**b**). Adapted with permission from [57]. Copyright 2001 American Chemical Society.

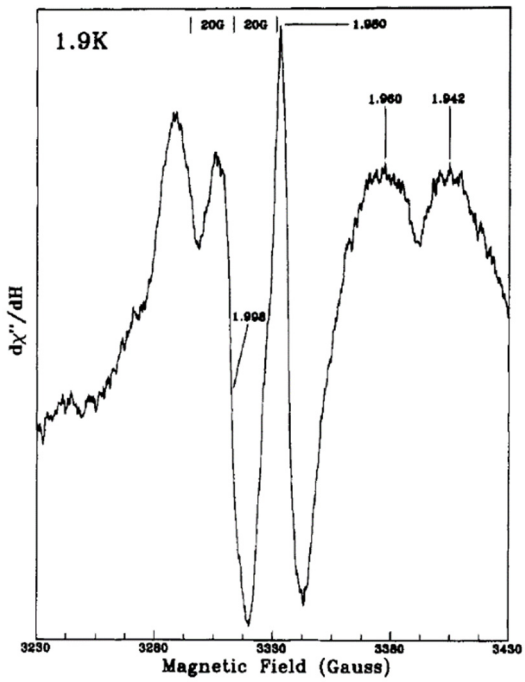

Figure 5. EPR spectra of degassed aqueous $Ti0_2$ colloidal solution after addition of 1 M methanol and irradiated at 1.9 K. Adapted with permission from [57]. Copyright 2001 American Chemical Society.

Coronado et al. [58] investigated the surface characteristics of anatase TiO_2 under UV Irradiation using EPR spectroscopy. At room temperature, the EPR spectrum of amorphous TiO_2 gel showed a signal with g_1 = 2.023, g_2 = 2.009, and g_3 = 2.004, which was very close to those corresponding to Ti^{4+}-O^{2-} species. It showed a broader signal as well with g = 1.93 of Ti^{3+} centers that were identical to those found in the spectra of colloidal TiO_2 after UV irradiation. On the other hand, the authors investigated the effect of the TiO_2 preparation method, i.e., hydrothermal and thermal, on EPR spectra. While the irradiated samples prepared by the hydrothermal method showed Ti^{3+} centers, only weak signals associated with oxygenated radicals were observed for the samples prepared by the thermal method. They found that after UV irradiation of crystalized TiO_2 at 77 K under vacuum, the signal at g > 2.00 that corresponds to Ti^{4+}-O^{2-} species were overlapped. However, a narrow signal with g = 1.990 and g_{II} = 1.960 was observed, which could be related to the electrons stabilized in Ti cations located at crystallization defects or at surface sites $(O^{2-})_x$-Ti^{3+}-$(OH^{-})_y$. In another experiment, the authors examined the EPR spectra of irradiated samples after the adsorption of oxygen. As oxygen is considered as an electron scavenger competing effectively with recombination, a higher amount of radicals was formed in this case. The simulation of the spectra has revealed three or four overlapping signals according to the sample examined. They assigned the signal at g_1 = 2.024, g_2 = 2.013, and g_3 = 2.003 to photogenerated holes trapped by subsurface lattice oxygens, giving O^{-} species. They explained that the signal of Ti^{3+} ions was located at the surface or within a few monolayers of the surface because of their rapid suppression upon the introduction of oxygen. Interestingly, Paranelli and coauthors have clarified the hole trapping sites' nature in the anatase polymorph by coupling CW-EPR and ENDOR (pulse electron-nuclear double resonance) techniques [59]. In their studies, the surface and subsurface holes in anatase were discriminated, in which the interaction of surface trapped holes with surface adsorbed water molecules was first measured using ENDOR. Water molecules play an important role in stabilizing the surface hole centers, where a complex environment composed by both surface hydroxyl groups and less close physisorbed water molecules are necessary.

Chiesa et al. [39] used CW-EPR spectroscopy to study charge carrier trapping in anatase and rutile TiO_2 polymorphs, in which they irradiated fully dehydrated samples kept under vacuum. At 77 K, photogenerated electrons gave an EPR signal at g_{II} = 1.962

and g_I = 1.992, which had been assigned to trapped electrons on lattice titanium ions. However, they clarified that the trapped hole signal can be related to at least two akin species with similar but distinct parameters. These holes were trapped at the surface since they reacted with molecular hydrogen acting as a hole scavenger. One dominant species of trapped holes appeared at g_1 = 2.027, g_2 = 2.015, g_3 = 2.003.

Yan et al. [60] studied the photoinduced electron-trapping states of anatase TiO_2 nanoparticles in two anaerobic systems, i.e., a proton-free system consisting of iodide ions in acetonitrile as a hole scavenger, and a protonated system consisting of methanol as a hole scavenger. Under UV illumination TiO_2 nanoparticles in the methanolic system exhibited a broad visible absorption peak at 725 nm and blue color of the electron-trapping state on TiO_2 nanoparticles (Figure 6a). In contrast, low absorption from 400 to 600 nm was observed in the LiI/MeCN system related to the absorption spectra of I^{3-} that was formed due to the oxidation of I^- by photoinduced holes (Figure 6b). EPR spectroscopy was then used to detect $^{\bullet}O^{2-}$ radicals produced under UV illumination from the reaction between O_2 and TiO_2 nanoparticles in different systems ($O_2 + e_{CB}^- \rightarrow {}^{\bullet}O^{2-}$). The authors only detected $^{\bullet}O^{2-}$ signals in the methanol system, indicating that photoinduced electrons under the proton-free condition are not able to react with O_2 to produce $^{\bullet}O^{2-}$ radicals. They used then low-temperature (4 K) EPR spectroscopy to distinguish the different photoinduced electron-trapping states on TiO_2 nanoparticles. As shown in Figure 6c, a rapid increase of a signal at g = 1.979 in systems containing methanol, ethanol, or acetonitrile was observed, in addition to a weak signal at g = 1.930 that appeared after 4 h of irradiation. While the first signal can be attributed to surface distorted four-coordinate tetrahedral Ti_{4c}^{3+} species, the latter can be assigned to anatase surface six-coordinate octahedral Ti_{6c}^{3+} species. The authors, thus, explained that the use of different electron donors in the presence of protons allowed the photoinduced electrons to be trapped mainly as surface Ti_{4c}^{3+} species with some surface Ti_{6c}^{3+} species. However, in LiI/MeCN proton-free electron donor system (Figure 6d), only an increasing peak at $g_\perp$ = 1.990 corresponds to the anatase lattice octahedral Ti_{6c}^{3+} state was observed. The authors, thus, explained that in the absence of protons, photoinduced electrons are trapped as interior interstitial Ti_{6c}^{3+} species in the lattice of the TiO_2 nanoparticles. The authors have finally concluded that the visible absorption signature at around 700 nm is dependent on the location of the trapped electrons, which can be controlled by protons' content. Hence, the presence of protons is required to induce the conventional blue coloration of TiO_2 in order to stabilize trapped electrons as surface Ti_{4c}^{3+} species.

Kumar et al. [61] studied in situ EPR for anatase (Hombikat UV100) and rutile TiO_2 nanoparticles under UV irradiation in air and vacuum conditions. The measurements were done at liquid helium (He) at a temperature of (4.2 K). EPR spectrum of anatase TiO_2 (Figure 7a) showed two signals, i. e., trapped electrons (signal A) at g_1 = 2.016, g_2 = 2.012, g_3 = 2.002 and $g_{|}$ = 1.958, $g_\perp$ = 1.988, and trapped holes (signal B) at g_1 = 2.016, g_2 = 2.012 and g_3 = 2.002. The authors assigned the sharp signal at $g_\perp$ and $g_{|}$ to surface electron trapping sites, while the latter signal was related to photogenerated holes trapped at the lattice oxygen atoms located in the subsurface layer as $Ti^{4+}O^{\bullet-}Ti^{4+}OH^-$ radical. Based on their observations, they suggested a charge-transfer mechanism in anatase TiO_2. On the other hand, EPR signals of rutile TiO_2 illuminated at 4.2 K (Figure 7b) were characterized by two sets of g values, $g_\perp$ = 1.969, $g_{|}$ = 1.947 (signal F) and g_1 = 2.019, g_2 = 2.014, g_3 = 2.002 (signal G). The authors have assigned signals F and G to the surface electron traps as Ti^{3+} and rutile hole trapping sites $Ti^{4+}O^{\bullet-}Ti^{4+}OH$, respectively. They noticed also a third signal (H) at g = 1.91 that was related to vacancy-stabilized Ti^{3+} in the lattice sites. The authors noticed also that the trapped electrons generated by irradiation at 4.2 K in anatase and rutile were stable below 85 K and vanished upon increasing temperature, while trapped holes are more stable up to ~150 K. Nevertheless, heating to ambient temperature showed the disappearance of hole trapping sites due to electron-hole recombination.

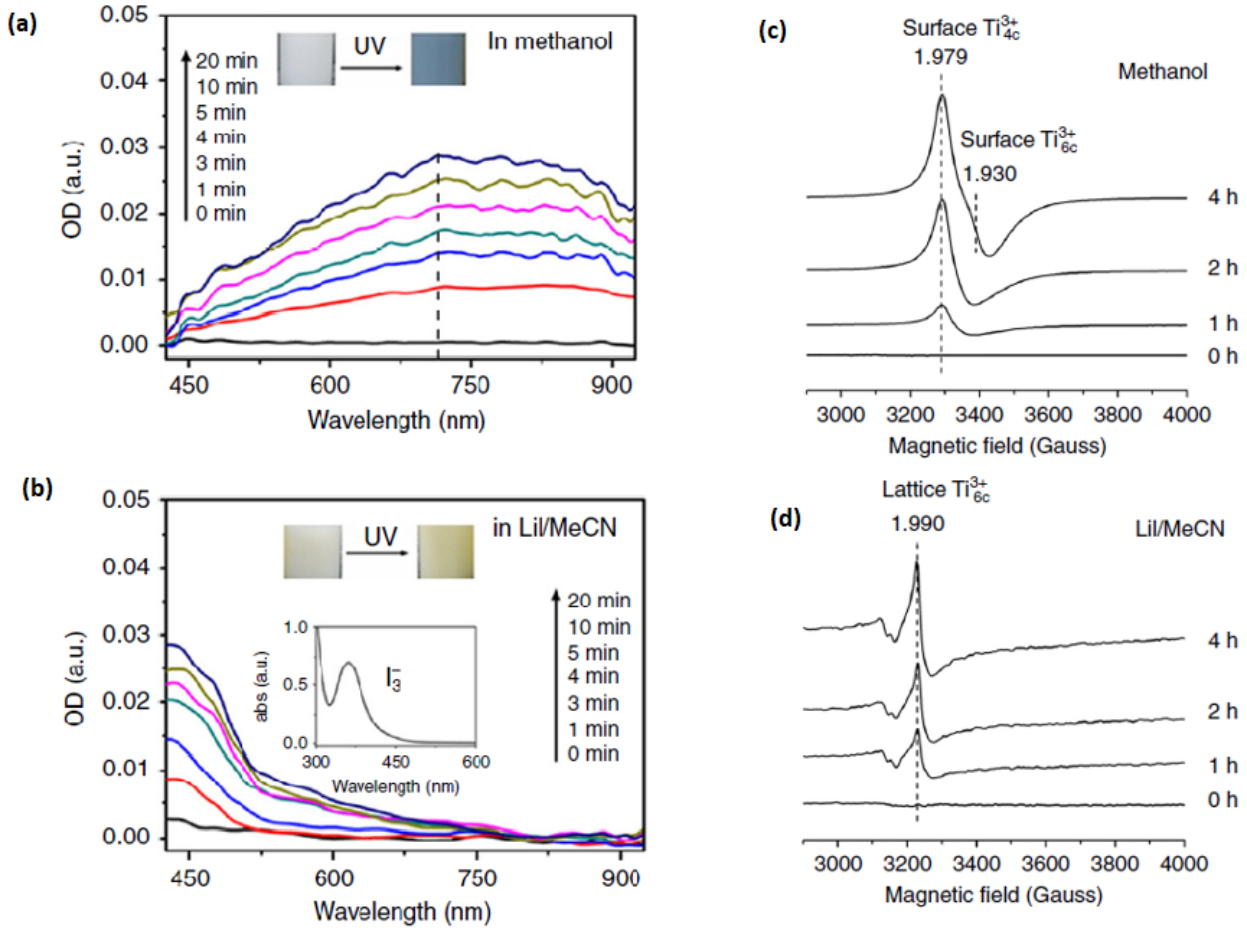

Figure 6. UV-vis absorption spectra (**a**) in methanol, (**b**) in LiI/MeCN. ESR spectra of TiO_2 nanoparticles in methanol under UV illumination (365 nm, 100 W) times (1–4 h) when TiO_2 nanoparticles were suspended (**c**) in 0.1M methanol solution and (**d**) in 0.1M LiI/MeCN solution. Reprinted from [60].

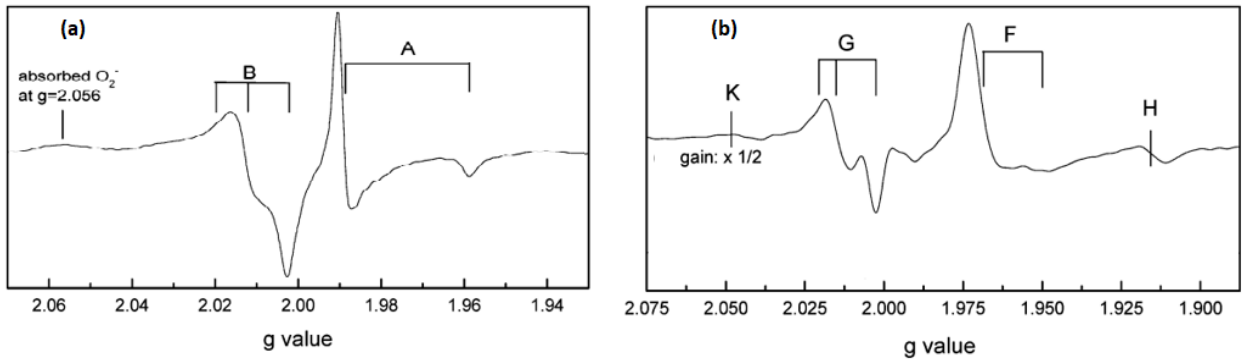

Figure 7. EPR spectra of (**a**) anatase and (**b**) rutile TiO_2 nanopowders at 4.2 K after 1 h of UV illumination. Adapted with permission from [61]. Copyright 2006 American Chemical Society.

In order to investigate the role of platinum as an electron scavenger on the surface of TiO_2, AlSalka et al. [21] investigated the paramagnetic centers produced upon the irradiation of self-prepared Pt/TiO_2 anatase powders via in situ EPR spectroscopy under an argon atmosphere at 77 K. In the presence of pre-adsorbed oxalic acid as a hole scavenger, the EPR spectra of irradiated Pt/TiO_2 showed two signals (Figure 8), weak signal H ($g > 2$) of trapped holes and signal ET ($g < 2$) of trapped electrons.

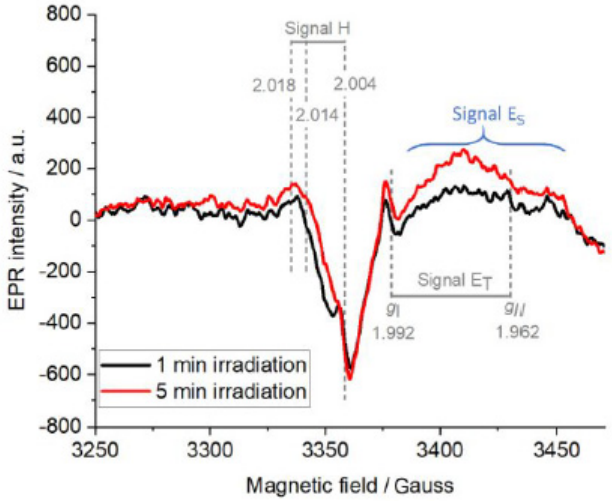

Figure 8. EPR spectra recorded when Pt/TiO_2 was irradiated for 1 min (black) and 5 min (red) in the absence of molecular oxygen at 77 K in the presence of oxalic acid. Reprinted with permission from [21]. Copyright 2020 American Chemical Society.

The authors assigned signal H (g_x = 2.004, g_y = 2.014, g_z = 2.018) to the photogenerated holes trapped near the hydrated anatase surface at the oxygen atoms in the form of Ti^{4+}-$O^{-\bullet}$-Ti^{4+}-OH-. In addition, they attributed signal ET (g_{II} = 1.962 and $g_{\perp}$ = 1.992) to the photogenerated electrons trapped in the bulk as Ti^{3+} ions. The authors clarified that the appearance of such a signal of trapped electrons even in the presence of platinum nanoparticles attached to the surface of TiO_2 can only be interpreted as not all the photogenerated electrons were scavenged by the loaded Pt NPs. Hence, not all the electrons can be used, thereafter, in reduction reactions, i.e., the hydrogen evolution reaction. Interestingly, the authors noticed another broad and unfeatured signal (ES) centered at 3450 gausses with increasing intensity over the irradiation time. They have explained this signal to the injection of electrons from $^{\bullet}CO_2^-$ radicals formed through the oxidation of oxalic acid by photogenerated holes, which can be then spread on the surface of TiO_2. Such a signal was also observed by Chiesa et al. [39] due to the excess electrons near the surface of anatase TiO_2 through the injection of electrons in the solid. Micic et al. [57] have also reported a broad asymmetric EPR signal at g = 1.981 of trapped electrons on the surface due to electron injection from methanol radicals into TiO_2 particles.

Al-Madanat et al. [62] compared the EPR spectra of 1.0 wt% Pt-loaded P25 and UV100 TiO_2 in the N_2 atmosphere to investigate the effect of the photocatalyst nature and PtNPs on the photogenerated electron and hole paramagnetic species. Upon illumination, both materials showed two main features shown in Figure 9a,b, i.e., the signals at g > 2.00 of the surface trapped holes and the signals at g < 2.00 of the trapped electrons. They explained that Pt-loaded UV100 showed the hole trapping site at g-tensor components g_x = 2.004, g_y = 2.015, and g_z = 2.019 that corresponds to the anatase oxygen site, while the small-signal at $g_{\perp}$ = 1.992 and the shoulder at g_{II} = 1.965 were related to the anatase lattice trapping electron site as Ti^{+3}. On the other hand, the signals of trapped holes in Pt-loaded P25 TiO_2 having g-tensor components g_x = 2.003, g_y = 2.019, and g_z = 2.026 were not completely resolved, considering a combination of trapped oxygen sites from anatase and rutile. However, the Ti^{+3} signal from anatase can be observed clearly at the same g-tensor components assigned for Pt-loaded UV100. Moreover, two other signals at $g_{\perp}$ = 1.980 and gII = 1.945 were attributed to Ti^{+3} sites for trapped electrons in the rutile lattice. The authors showed that around 20% higher relative intensity of trapped holes was noticed in Pt-loaded UV100, while Pt-loaded P25 had more intense signals of both trapped Ti^{+3} sites. In this case and because no hole scavenger was used, the authors believed that UV100 exhibited better electron transfer to Pt islands than P25, inhibiting the charge carriers' recombination and increasing the photocatalytic activity.

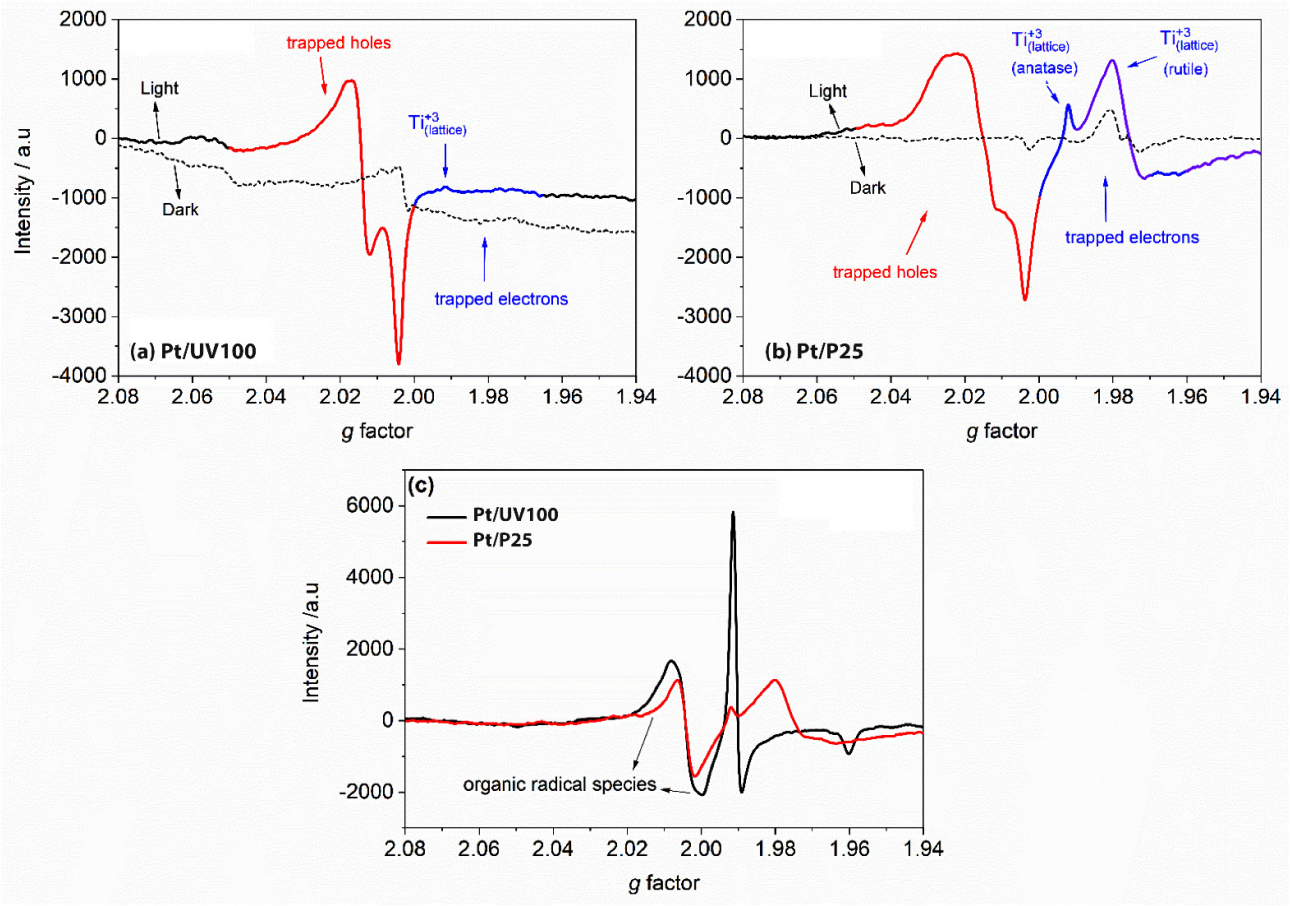

Figure 9. EPR spectra measured at 77 K in N_2 atmosphere for (**a**) Pt/UV100, and (**b**) Pt/P25 in dark and light. (**c**) The photogenerated signals for Pt/UV100 (black) and Pt/P25 (red) in the presence of N_2-naphthalene vapor under illumination. Adapted from [62].

The authors have then made the experiment in the presence of naphthalene to investigate the naphthalene radical cation generated through the reaction via single-electron transfer with photogenerated holes. Both materials as can be seen in Figure 9c produced similar EPR signals at $g_x = 2.002$, $g_y = 2.006$. However, Pt-loaded UV100 produced relatively higher signals of organic radicals and trapped electrons, which could be due to its better charge carrier separation.

Al-Madanat et al. [63] have also investigated the effect of platinum loading method on TiO_2, i.e., through photodeposition or physical mixing after the laser ablation, on the e^-/h^+ populations under irradiation in N_2 or N_2-methanol atmosphere using EPR spectroscopy and commercial TiO_2 (anatase UV100). As shown in Figure 10a, upon illumination, two groups of signals were recorded for all the materials used, the first at ($g_x = 2.004$, $g_y = 2.015$, and $g_z = 2.019$) and the second at ($g_{||} = 1.992$ and $g_{\perp} = 1.961$) and ($g_{||} = 1.961$ and $g_{\perp} = 1.94$–1.93), which were assigned to trapped holes at or near the surface and trapped electrons in the bulk and at the surface, respectively. In an inert atmosphere, Pt/TiO_2 prepared via the photodeposition method showed the strongest h^+ signal and the weakest e^- signal, indicating a better electron transfer to Pt than in the other samples. However, this was also evidence of the non-complete scavenging of electrons by Pt. In the N_2-methanol atmosphere (Figure 10b), a triple signal of the $^{\bullet}CH_2OH$ radical was produced with a simultaneous appearance of stronger signals of the trapped electrons attributed to the current doubling effect. Pt/TiO_2 prepared via the photodeposition showed again the smallest electron signal, confirming the best charge carrier separation among other samples, and thus the highest photocatalytic activity.

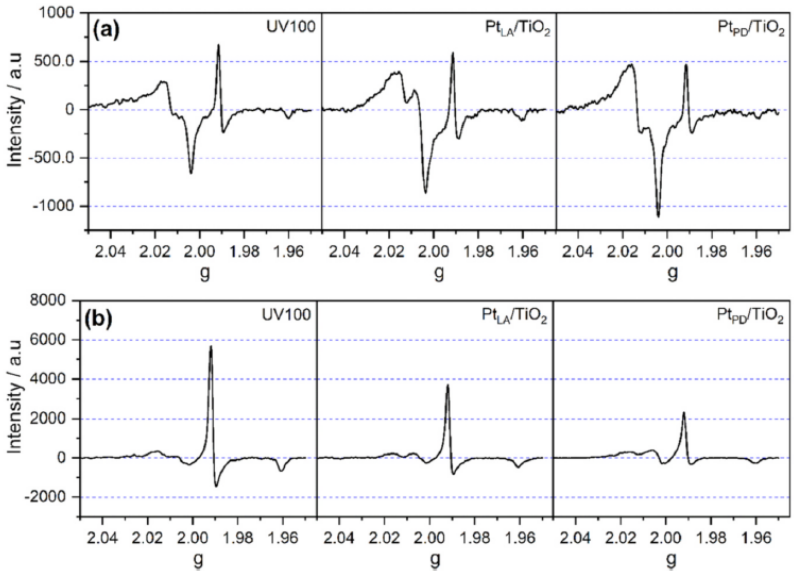

Figure 10. EPR signals of the trapped electrons and holes for pristine UV100 TiO_2 and Pt-loaded UV100 at 77 K in (**a**) N_2 and (**b**) methanol conditions. Irradiation time: 7 min. Reprinted with permission from [63].

3. Niobium(V) Oxide Photocatalyst

Apart from the TiO_2-based photocatalysts, Nb_2O_5 is also a widely used semiconductor oxide due to its properties such as thermal and chemical stability, and appropriate electronic and morphological properties for photocatalytic applications [64,65]. Nb_2O_5 is a polymorphic material with different crystalline phases related to the preparation conditions, with their structures formed by different arrangements of NbO_6 octahedra [66]. Its surface contains strong redox ability and both Lewis (LASs) and Brønsted acid sites (BASs), offering rich surface chemistry. In addition, the values of Nb_2O_5 bandgap energy are found to be between 3.0 and 3.4 eV, being suitable for photocatalytic reactions [67]. Similar to TiO_2, under excitation by suitable wavelength energy, an electron (e^-) is promoted to the conduction band (CB) while a hole (h^+) is formed in the valence band (VB). Nb_2O_5 has not been yet so deeply investigated by EPR but, in general, it does not present so many characteristic signals as observed in the literature for TiO_2. Nevertheless, the EPR technique can also bring up much insights about the processes on the surface of the photocatalyst. Some reported works have shown the presence of new states as Nb(IV) centers or oxygen vacancies by using EPR measurements on doped Nb_2O_5 [68,69]. Besides, Nb_2O_5 photocatalyst can also be combined with other materials, including TiO_2, to promote better efficiencies. One work regarding the heterojunction of TiO_2 and Nb_2O_5 was reported by Li and coworkers [70]. The authors prepared ultra-fine niobium oxide nanoparticles on the surface of rutile TiO_2 and evaluated their different proportions and activities for photocatalytic oxidation of phenylethanol and methanol photoreforming. They investigated the prepared materials employing EPR (Figure 11). Under dark conditions, no signal was detected for pure Nb_2O_5 but one weak peak (g = 2.001) was observed for pure rutile TiO_2 and Nb_2O_5/TiO_2 composites which attributed to O^- formed from O_2 onto the surface. In addition, when the proportion of Nb_2O_5 in the Nb_2O_5/TiO_2 composites was increased, the intensity of this signal decreased, indicating that Nb_2O_5masked the defect sites of TiO_2, which seemed to work as nucleation centers for niobium oxide. When the samples were exposed to UV-vis irradiation, typical EPR signals assigned to superoxide species (g_1 = 2.002, g_2 = 2.009, g_3 = 2.028) were identified. The authors reported that more superoxide species were produced on Nb_2O_5/TiO_2 heterojunctions. Furthermore, two signals corresponding to the bulk Ti^{3+} species (g = 1.982 and 1.978) were also found higher for the heterojunction. These facts evidence a better charge separation efficiency for the composite's materials.

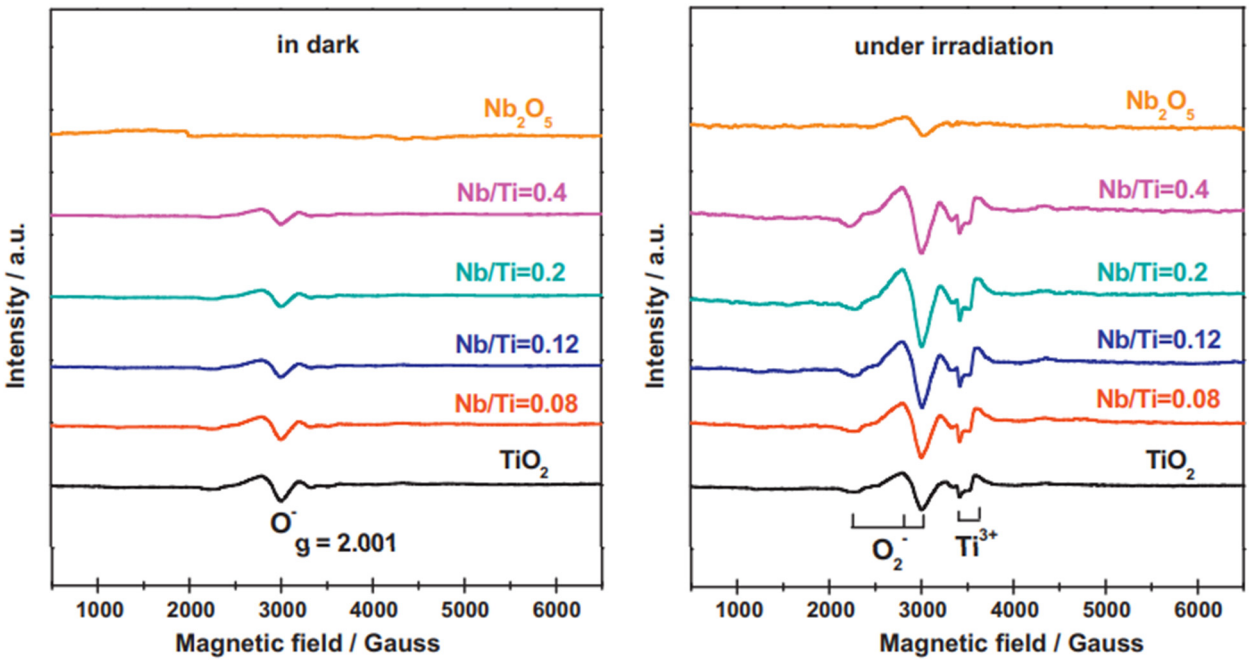

Figure 11. EPR spectra of TiO_2 and Nb_2O_5/TiO_2 heterojunctions in the dark and under irradiation at 100 K after the evacuation of the samples. Reprinted with permission from [70].

The group of Tanaka and coworkers performed many EPR studies towards the surface of Nb_2O_5 when applied for organics photooxidation. Firstly, they explore the photooxidation of alcohols at low temperatures and in organic solvent-free conditions by using niobium oxide in an oxygen atmosphere [71,72]. The prepared Nb_2O_5 was identified as TT phase (a kind of Nb_2O_5 phase) and a pseudohexagonal structure. A remarkable result observed by the author was the photooxidation of 1-pentanol under irradiation up to 480 nm, even though bare Nb_2O_5 is not able to absorb wavelengths higher than 390 nm. This fact could indicate that the photooxidation occurred by a different pathway rather than the expected electron transfer from the excited semiconductor. Based on EPR investigations, in Figure 12, the mechanism for 1-pentanol photooxidation was then clarified. Firstly, when Nb_2O_5 was irradiated in presence of an excess of 1-pentanol (123 K), a broad ESR signal assigned to Nb^{4+} (g = 1.9) was observed (Figure 12c). In the presence of O_2, this signal disappeared, indicating that Nb^{4+} was oxidized to Nb^{5+} (Figure 12d). Other EPR analyses showed a signal related to alkenyl radical (g = 2.006, A_{H1} = 2.0 mT, A_{H2} = 4.4 mT) which was not significantly affected by the addition of O_2. Besides, no oxygen anion radicals were detected, supporting the selectivity of the reaction. The mechanism of 1-pentanol to produce carbonyl compound was correlated to an electron transfer from the absorbed alcoholate to Nb_2O_5 forming Nb^{4+} centers. The alcoholate was further converted to the carbonyl compound and the Nb^{4+} sites are reoxidized to Nb^{5+} by the molecular oxygen.

Similarly, the authors further studied the partial photooxidation of hydrocarbons by Nb_2O_5 and also compared its efficiency with TiO_2 [73]. In principle, Nb_2O_5 showed higher selectivity than TiO_2 for some hydrocarbons such as cyclohexane and ethylbenzene. At this time, no significant activity was observed under visible light irradiation showing that the photooxidation mechanism involves the Nb_2O_5 excitation. The EPR analysis (77 K) at first showed the formation of O_2^- species from absorbed O_2 by excited electrons on the oxide. Then, when ethylbenzene was adsorbed on Nb_2O_5 and exposed to irradiation, signals related both to ethylbenzyl radical (g = 2.003, A_{H1} = 6.0 mT, A_{H2} = 2.0 mT) and Nb^{4+} centers (g = 1.933) were observed. These results could support the proposed mechanism in which the benzylic C–H bond of ethylbenzene was oxidized by the photogenerated hole while the excited electrons formed the Nb^{4+} centers. When the sample was exposed to O_2, the signal for ethylbenzyl radical vanished and the oxygen radical was detected,

indicating the formation of diamagnetic alkyl peroxide anion (ROO^-) or hydroperoxide (ROOH). Along with other analyses, the suggested mechanism was based on the oxidation of alkyl radical to alkyl hydroperoxide and then, after protonation, the alkyl hydroperoxide produced ketone and water. The higher selectivity found for Nb_2O_5 was related to the lower amount of oxygen radicals and also to the absence of O_3^- species which are strong oxidizing radicals when compared to TiO_2.

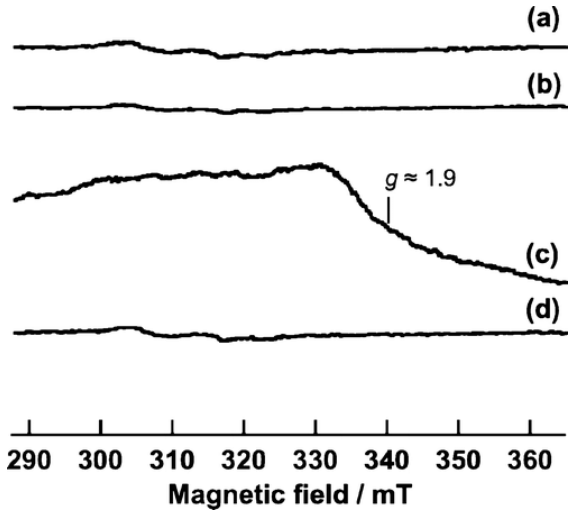

Figure 12. EPR spectra of Nb_2O_5 (**a**) after pretreatment, (**b**) in the dark and (**c**) under UV irradiation in the presence of 1-pentanol, and (**d**) after the introduction of O_2. Pretreatment: evacuation at 773 K for 1 h followed by oxidation at 773 K with 10.7 kPa of O_2 and then evacuation at 773 K for 1 h. Reprinted with permission from [71]. Copyright 2009, American Chemical Society.

The group also showed an effective photoactivity by LMCT (ligand to metal charge transfer) transitions between small aromatic hydrocarbons and the surface of Nb_2O_5 [74]. The material was able to selectively photooxidative hydrocarbons to carbonyl compounds under visible light irradiation. In this case, a pre-treatment was performed; the catalyst powder was first evacuated and then heated (573 K) in a reactor in situ, which showed enhanced activity for toluene photooxidation with high selectivity. In principle, the treatment did not affect the Nb_2O_5 structure as the surface area, crystal phase, and crystallinity, and just a very slight change was observed in the UV-vis spectra. In fact, the enhanced photoactivity was explained by the toluene adsorption on treated Nb_2O_5 which generated an additional visible light absorption. This transition was related to an LMCT from toluene to Nb^{5+}. Interestingly, the same phenomenon was not observed for TiO_2 even when the pre-treatment was applied. In the case of toluene as an electron donor, it was assumed that Nb_2O_5 had a higher affinity to the electrons in comparison to TiO_2. In the EPR measurements (77 K), the treated Nb_2O_5 in absence of toluene did not show any signal also under visible light irradiation. In contrast, when toluene was absorbed on Nb_2O_5 surface, a EPR signal was observed and assigned to toluene radical cation (g = 2.003, A_{CH3} = 0.58 mT, $A_{H2,6}$ = 0.81 mT, $A_{H3,5}$ = 0.59 mT, and A_{H4} = 0.78 mT), which was confirmed by a simulated spectrum as shown in Figure 13. At this time, the authors did not observe the signal related to Nb^{4+} formation. They suggested that the excited electrons would be delocalized in the conduction band of the oxide. When the sample was exposed to O_2 in the dark, the intensity of the toluene radical signal did not change; evidencing that O_2 itself could not oxidize toluene. Thus, the mechanism was based on the formation of superoxide radicals from the excited Nb_2O_5, which provoked the cleavage of the benzyl C−H bond of the toluene radical cation to form benzyl ($Ph-CH_2^{\bullet}$) and hydroperoxyl ($^{\bullet}OOH$) radicals. In sequence, the benzyl radical was converted to benzylperoxy radical by the intercalation of adsorbed O_2. The main product of the toluene photooxidation was found to be benzaldehyde.

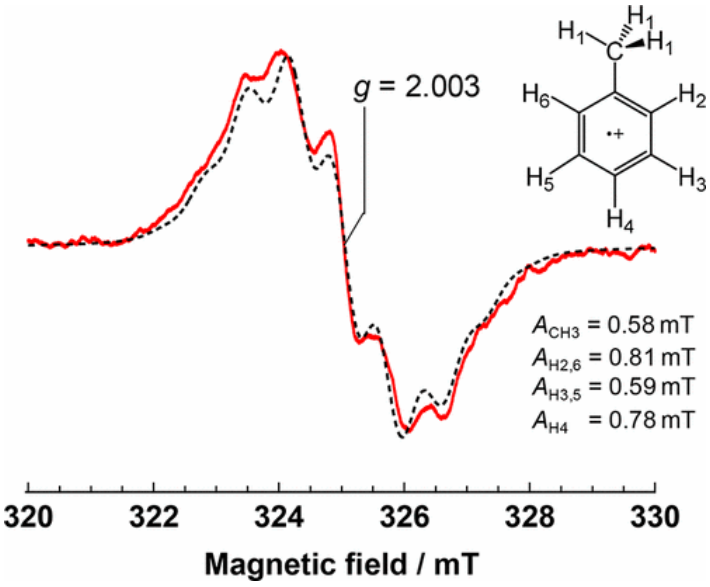

Figure 13. EPR spectrum of adsorbed toluene on Nb_2O_5 after visible light irradiation (red solid line) and simulated spectrum of toluene cation radical (dash line). Simulation parameters are shown in the inset. Reprinted with permission from [74].

Other organic compounds also investigated by Tanaka's group for selective photooxidation over Nb_2O_5 were amines [75]. Similar to the previous works, the reaction to produce imines was active under visible light irradiation. This time, the mechanism was related to the adsorbed amine on Nb_2O_5 which gave rise to a donor level localized in the nitrogen from the amine species. In the EPR analysis (77 K), under visible light irradiation, the spectrum of Nb_2O_5 in presence of butylamine showed signals related to both the organic radical (g = 2.005) and Nb(IV) (g ~ 1.92). Based on this result and some DFT calculations, it was explained that the photoactivation of the surface complex formed by the amine and Nb_2O_5 occurred via an electronic transfer from the N 2p orbital to the Nb 4d orbitals from the oxide conduction band. Thus, the amine oxidative dehydrogenation to form imine was based on the photoexcitation of the Nb_2O_5−amide surface complex which was active under visible light.

4. Spin Trapping in the Liquid Phase

After the pioneering works of Janzen et al. in 1969 [76] and Lagercrantz in 1970 [77], the free radical trapping technique "spin trapping" has been intensively introduced as a valuable tool in different fields, such as chemistry, physics, biology, and medicine for the detection and identification of the transient radicals formed in the reaction system [78–82]. Since these formed radicals have a very short lifetime usually nanoseconds half-lives, the base of this method is to add a new diamagnetic reagent; spin trap agent, to the reaction medium which reacts with these radicals producing a new and more stable persistent paramagnetic species "spin adduct" that can be registered, qualified and quantified by the electron paramagnetic spectroscopy (EPR), Scheme 5 [76,83].

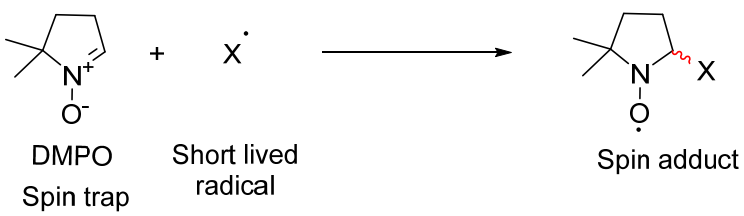

Scheme 5. Illustration of the spin trapping method.

Nitroso and nitrone derivatives have been widely used as the main types of spin trapping agents (Chart 1). The former is characterized by the faster trapping rate and trapping the carbon-center radical, while, the latter is more suitable for trapping the oxygen-centered radicals [84,85]. However, due to the limitations of the linear nitrone to facilitate the identification of the trapped radicals, new spin traps based on pyrroline N-oxide derivatives have been developed [85,86].

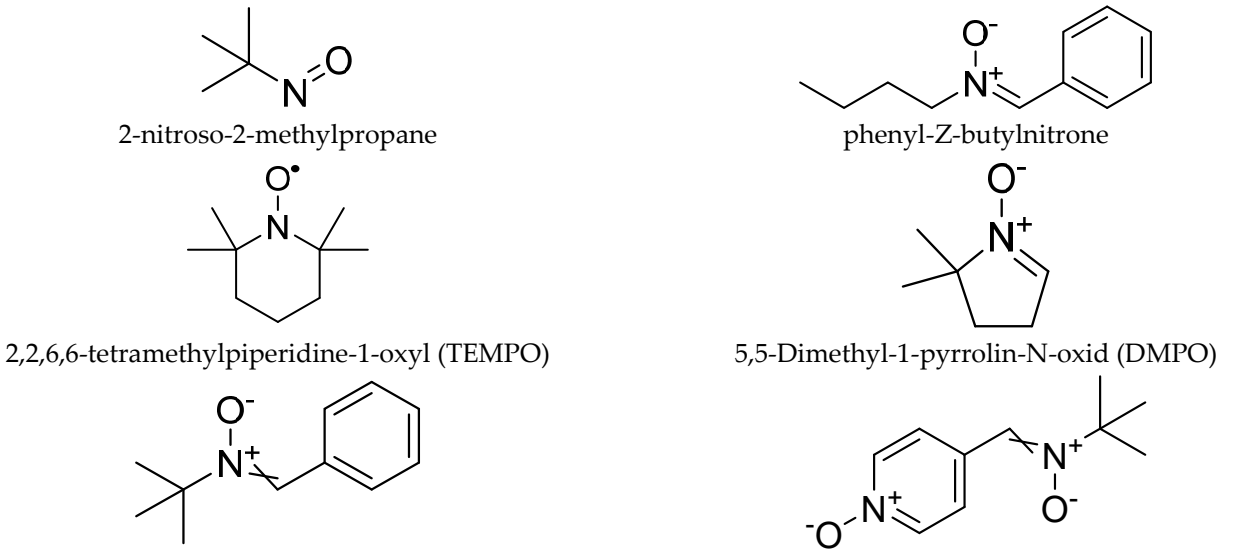

Chart 1. The chemical structure of different kinds of EPR spin trapping agents.

Recently, the spin trapping technique is widely employed in the photocatalytic reaction as a valuable tool to study the reaction mechanism [21,87]. Among several spin traps agents, such as 2,2,6,6-tetramethylpiperidine-1-oxyl (TEMPO), 4-hydroxy-5,5-dimethyl-2- trifluoromethylpyrroline-1-oxide (FDMPO), α-(4-pyridyl-1-oxide)-*N*-*tert*-butyl nitrone (POBN), and N-tert-butyl-a-phenylnitron (PBN), 5,5-Dimethyl-1-pyrrolin-N-oxid (DMPO) is the most used spin trap due to the well resolved and characteristic EPR spectra with the superoxide and hydroxyl radicals [10,86–88]. Figure 14 shows the EPR spectra for the DMPO-OH and DMPO-O_2 adducts after the reaction of the hydroxyl radicals and superoxide with DMPO under irradiation.

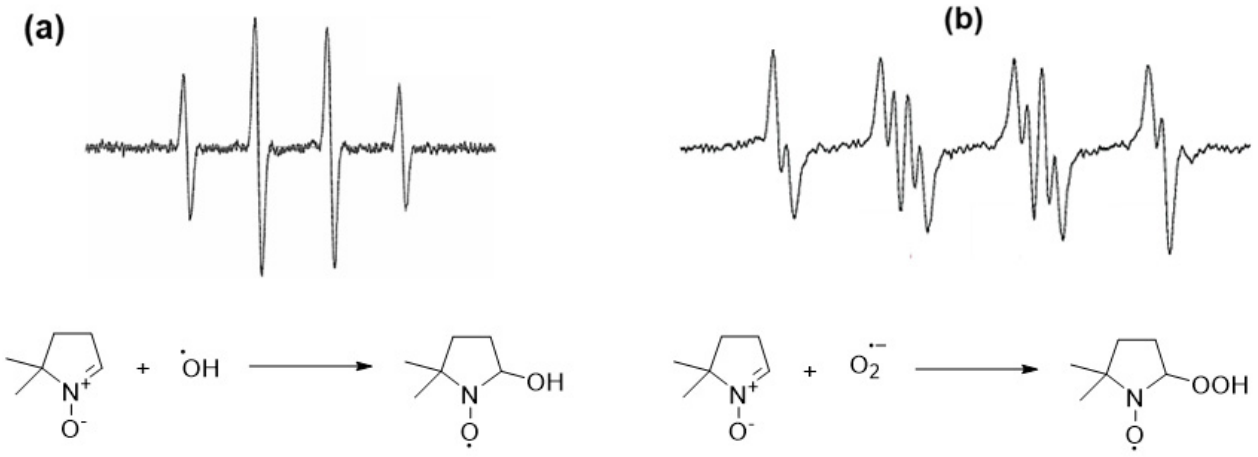

Figure 14. EPR spectra of the diamagnetic adduct formed after the reaction of DMPO with (**a**) hydroxyl radical (•OH), (adapted with permission from [87], Copyright 2020, American Chemical Society) and (**b**) superoxide radical ($O_2^{\bullet-}$) (adapted with permission from [89], Copyright 2005, American Chemical Society).

In the photocatalytic process over TiO_2, it has been frequently claimed that the hydroxyl radical is produced during the irradiation of an aqueous TiO_2 suspension through the decomposition of the water molecule by the photogenerated hole (Equations (27) and (28)). The hydroxyl radical was introduced as the most important reactive species "oxidant" generated during the photocatalysis process.

$$TiO_2 \xrightarrow{hv} TiO_2\left(e^- + h^+\right) \quad (27)$$

$$h^+ + H_2O \rightarrow H^+ + {}^{\bullet}OH \quad (28)$$

Besides, in the presence of molecular oxygen (O_2) in the photocatalytic system, it is likely that the adsorbed O_2 on TiO_2 surfaces will react with the conduction band photogenerated electron to produce superoxide radicals (perhydroxyl radical), according to Equations (29) and (30).

$$e^- + O_2 \rightarrow O_2^{\bullet -} \quad (29)$$

$$O_2^{\bullet -} + H^+ \leftrightarrow HO_2^{\bullet}\ (pKa = 4.8) \quad (30)$$

Jaeger and brad [90] employed the spin trapping technique to detect the formed free radical species in situ during the irradiation of the aqueous suspension of TiO_2 and Pt-TiO_2 (anatase) in the presence of the spin traps PBN or POBN at room temperature. The authors did not observe any EPR signal in the dark, however, immediately after the illumination of the TiO_2 suspension with a light (>3.2 eV), the EPR signal was observed in the presence of both spin traps. The authors attributed the signal in the PBN\TiO_2 system to the formation of 4 different paramagnetic species. Two of them was assigned to the formation of the ${}^{\bullet}OH$ and $HO_2^{\bullet}$ (perhydroxyl radical). Although the authors are not certain from the origin and kind of the others two species, they are suggested that these species are formed due to the decomposition of t+he spin trap. Moreover, by using the spin trap POBN at different pH (4, and 7), they confirmed the formation of the ${}^{\bullet}OH$ and $HO_2^{\bullet}$ species. On the other hand, using the pristine TiO_2 instead of the Pt-TiO_2 leads to the formation the ${}^{\bullet}OH$ and $HO_2^{\bullet}$, however, their concentrations are lower than that in the case of Pt-TiO_2.

Several research groups have been explored the photocatalytic activity, as well as the photocatalytic mechanism involved in the presence of different photocatalysts employing the EPR spin trapping techniques [19,21,86–88,91]. Fu et al. [92] investigated the photocatalytic degradation of 4-chlorophenol (4-CP) using N-doped TiO_2 prepared by the high-temperature nitridation of commercial P25 (Degussa) and undoped P25-TiO_2 annealed with N_2 in the same process as a reference sample, under UV and visible light ($\lambda > 420$ nm). The authors observed that P25-TiO_2 exhibited higher activity for 4-CP decomposition than that of N-doped TiO_2, while, under visible light irradiation, P25-TiO_2 did not exhibit photocatalytic activity for degradation of the 4-CP degradation, since it was not visible-light active material. The degradation of 4-CP, however, was observed from N-doped TiO_2, suggesting that N doping for TiO_2 is an effective approach for achieving visible-light-driven photocatalysis.

To explain the different activities between the studied materials the authors employ the ESR spin-trap technique using DMPO, to monitor the intermediate radicals and probe the nature of the reactive oxygen species generated during the UV and visible light irradiation in both systems. No EPR signals were observed by the authors in the dark in the presence of the catalysts or when 4-CP was absent (Figure 15). Under UV irradiation, the signal of DMPO−OH adduct (quartet peaks with a 1:2:2:1 intensity) was observed after a 20 s of illumination, and its intensity further increased after 80 s of irradiation in the presence of both photocatalysts, however, the peak intensity of DMPO−OH adduct generated by N-doped TiO_2 was less than that of TiO_2, suggested that the lower production of ${}^{\bullet}OH$.

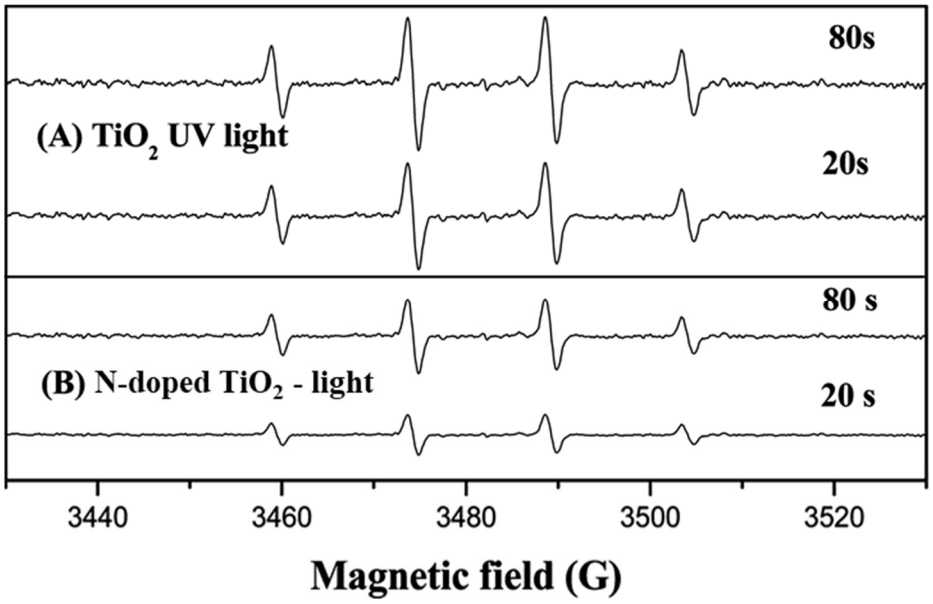

Figure 15. DMPO-OH spectra under UV irradiation in 4 CP aqueous suspension with (**A**) P25-TiO_2, (**B**) N-doped TiO_2: catalyst loading, 0.5 g L^{-1}; 4-CP concentration, 10 mg L^{-1}; DMPO concentration, 1.6×10^{-2} M. Reprinted with permission from [92]. Copyright 2006 American Chemical Society.

In the previous experiments, although the formation of the superoxide radical ($O_2^{\bullet -}$) was expected through the scavenging of the conduction band electrons by O_2, the authors did not observe such signal. They explained that to the instability of this radical in the aqueous medium, where it reacts with the present proton (Equation (31)) to produce H_2O_2 and O_2 ($k = 6.6 \times 10^3$ M^{-1} s^{-1}), due to the slow reactions between $^{\bullet}OOH/O_2^{\bullet -}$ and DMPO ($k = 10$ M^{-1} s^{-1}). Therefore, they performed the same experiment in an ethanolic medium to confirm the formation of DMPO-$^{\bullet}OOH/O_2^{\bullet -}$, and they observed a similar trend to the $^{\bullet}OH$ production in both systems.

$$2\,O_2^{\bullet -} + 2\,H^+ \quad \rightarrow \quad O_2 + H_2O_2 \tag{31}$$

On the other hand, when 4-CP/N doped TiO_2 suspension in H_2O and ethanolic solution irradiated with visible light, both DMPO-OH and DMPO-OOH adducts were registered, respectively, and the EPR signal intensity was enhanced gradually with increasing illumination time (Figure 16). However, the signal intensities were found weaker than those under UV light. Based on these results, the authors concluded that the photocatalytic degradation of 4-CP over N-doped TiO_2 under UV or visible light occurs in a similar mechanism, mainly by the radical reaction, which is similar to TiO_2 under UV light irradiation. According to the EPR results, the authors considering that the formation of DMPO-OH/OOH adducts give direct evidence that ($^{\bullet}OH$ and $O_2^{\bullet -}$) are the main active species responsible for the photodegradation of 4-CP, strongly suggesting that the photocatalytic reaction of organic compounds over N-doped TiO_2 proceed via surface intermediates of oxygen reduction or water oxidation (indirect path), not via direct reactions with holes trapped at the N-induced midgap level.

To better understand the interfacial interactions between the acetate and the TiO_2 at different pH, Belhadj et al. [88] investigated the adsorption and the photocatalytic degradation of acetate on anatase surface (UV100) by combining the EPR and attenuated total reflection Fourier transform infrared (ATR-FTIR) techniques. In this study, the authors employed DMPO as a spin trap to probe the formed reactive oxygen species during the photocatalytic degradation of acetate in H_2O and D_2O under aerobic conditions at different pH. At pH 6.0 in H_2O and pD 6.4 in D_2O, similar EPR signals were registered under the UV(A) irradiation in the presence of DMPO (Figure 17), which was attributed to the formation of DMPO-OH and DMPO-OD adducts, respectively. While, at pH 9 in H_2O, a

stronger signal for DMPO-OH was only registered (Figure 18a). In contrast, a different EPR signal containing several peaks was observed at pH 3 (Figure 18b). A negligible DMPO-OH signal was formed at pH 3 compared to that at pH 9. The authors attributed this signal to the formation of different DMPO adducts; i.e., DMPO-OH, DMPO-OOH, and DMO-OCH_3. Based on these results and the ATR-FTIR result, the authors suggested that the photocatalytic degradation of acetate at pH 9 mainly occurred by indirect oxidation by the $^{\bullet}$OH attack, as it is being predominately formed by oxidation of the adsorbed hydroxyl ions on the TiO_2 surfaces. On the other hand, the formation and the increase of DMPO-OCH_3 adduct signal during the irradiation at pH 3 suggested that the photooxidation of acetate occurs mainly through direct oxidation by the hole (h^+). These results show the existence of different radical intermediates at different pH, which would provide new insight into the mechanism of the oxidation of acetate at different pH.

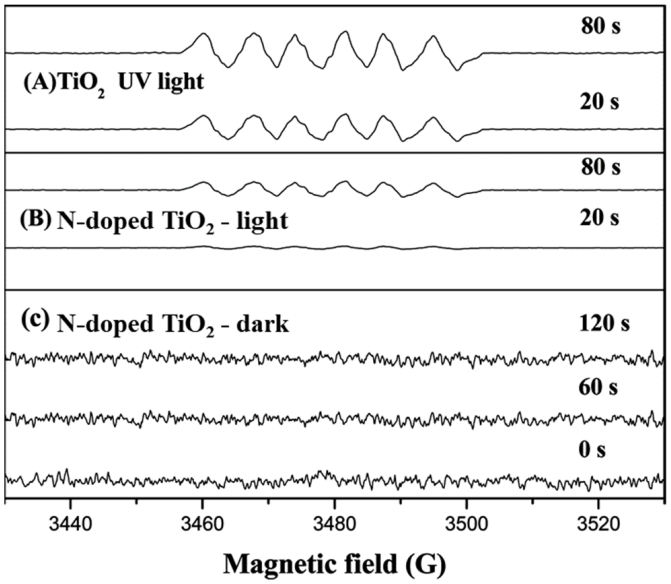

Figure 16. DMPO-$^{\bullet}$OOH spectra under UV irradiation in 4 CP ethanolic solution with (**A**) P25-TiO_2, (**B**) N-doped TiO_2 and (**C**) N-doped TiO_2 in dark: catalyst loading, 0.5 g L^{-1}; 4-CP concentration, 10 mg L^{-1}; DMPO concentration, 1.6 × 10^{-2} M. Reprinted with permission from [92]. Copyright 2006 American Chemical Society.

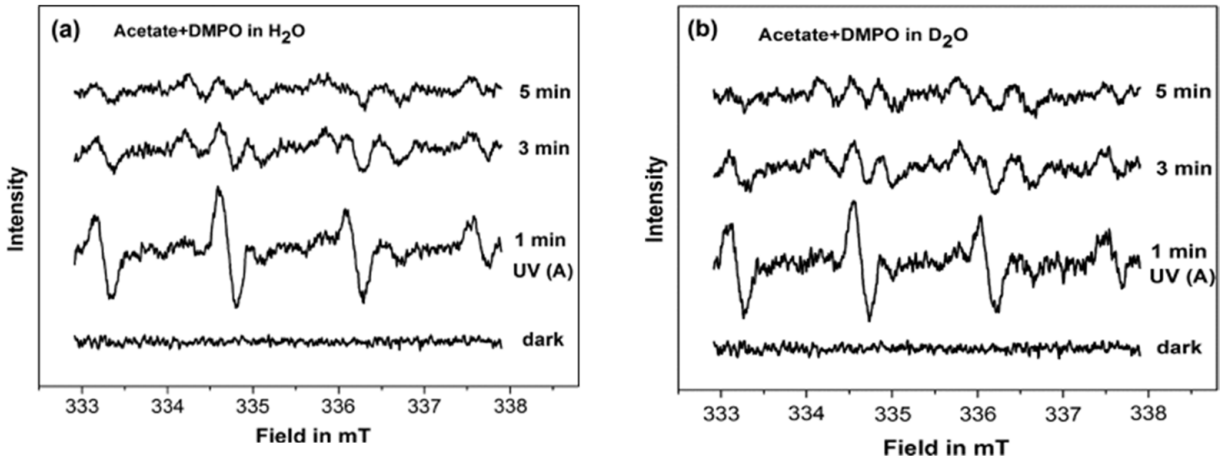

Figure 17. DMPO spin-trapping EPR spectra in the dark and under UV(A) irradiation at (**a**) pH 6.0 in H_2O, and (**b**) pD 6.4 in D_2O. Reprinted with permission from [88].

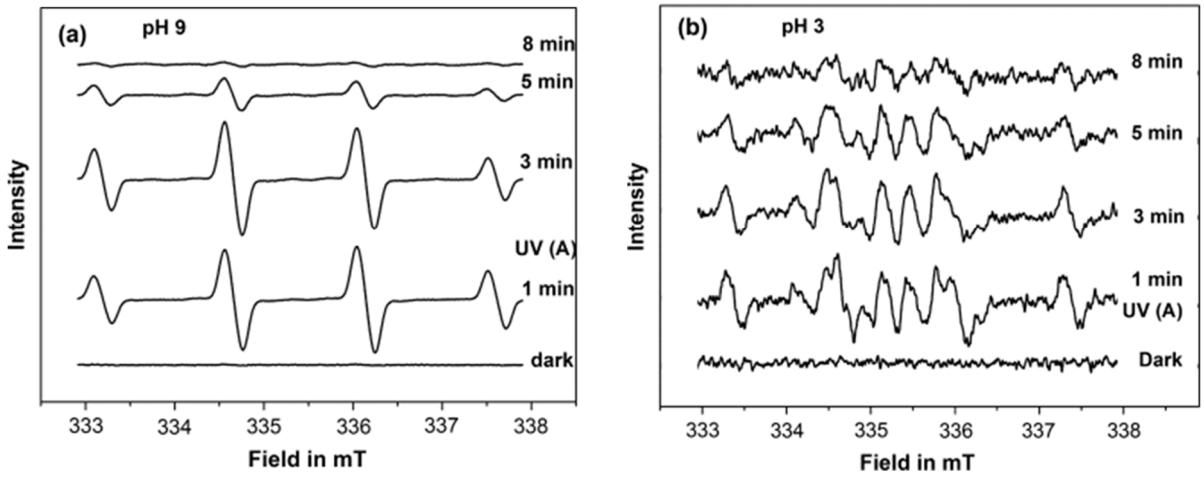

Figure 18. DMPO adducts EPR spectra in the dark and under UV(A) irradiation at (**a**) pH 9, and (**b**) pH 3. Reprinted with permission from [88].

Although the EPR spin trapping has been always considered as a useful technique to confirm the involvement of the hydroxyl radical in the photocatalytic process, however, this technique can be also used to confirm the opposite. Al-Madanat et al. [87] employed this technique during the study of the photocatalytic mechanism of naphthalene reforming over Pt-TiO_2 (UV100, anatase) to obtain additional insights regarding the role of $^{\bullet}OH_{free}$ in the photocatalytic reforming process. In this study, the authors performed the photocatalytic reforming reaction of naphthalene in the presence of two scavengers, potassium iodide (KI) as a hole scavenger and 2-methylpropan-2-ol ($(CH_3)_3COH$, TBA) as a hydroxyl radical ($^{\bullet}OH$) scavenge to determine the involvement of different active species in the photoreforming process. They found that the conversion of naphthalene is completely inhibited in the presence of KI. while, the addition of TBA does not affect the photocatalytic process, which suggested that the presence of free hydroxyl radicals ($^{\bullet}OH_{free}$) has a very limited contribution in the naphthalene conversion. To prove that, they performed the photoreforming naphthalene in the presence of either TBA or KI and DMPO. The authors observed the formation of DMPO−OH adduct in all the detected samples, as shown in Figure 19.

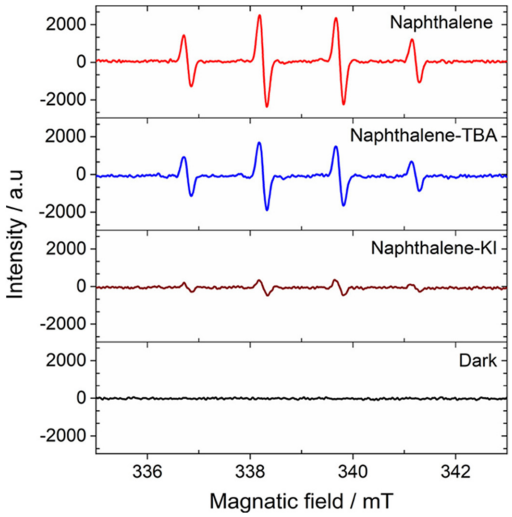

Figure 19. EPR spectra recorded during the photocatalytic reforming of naphthalene after 15 s in the presence of DMPO, DMPO–TBA, and DMPO–KI. [Catalyst], 1 g L^{-1}; 156 µmol L^{-1} aqueous solution of naphthalene; 20 mmol L^{-1} of KI and TBA; microwave frequency, 9.51 GHz. Reprinted with permission from [87]. Copyright 2020 American Chemical Society.

However, the authors observed that in the presence of TBA the adduct signal shows a decrease of 35%, confirming •OH-scavenging properties of TBA. Nevertheless, this lower quantity of available •OH radicals do not impact degradation of naphthalene as the authors mentioned before according to the scavenger experiments, providing evidence against a degradation mechanism initiated by the attack of $^{\bullet}OH_{free}$. On the other hand, the addition of KI to the system practically nullifies the adduct formation, as could be expected from the efficient hole consumption by this scavenger. Therefore, according to these results, the authors excluded the involvement of the $^{\bullet}OH_{free}$ in the degradation of naphthalene during the photocatalytic process.

The EPR spin trapping technique was also used to study the mechanism of the photocatalytic reaction in the presence of other reactive species than the •OH and $O_2^{\bullet-}$ radicals such as $^{\bullet}CO_2^-$ [93,94] and organic radicals [22,23,95]. Besides, it was also used to confirm the activity differences between the employing photocatalysts [21,96]. Alsalka et al. [21] studied the photocatalytic reforming of oxalic acid employing self-prepared TiO_2 photocatalysts loaded with different noble metals (Pt and/or Au). By using DMPO as a spin-trapping agent, the authors traced the nature of the photogenerated species during the oxalic acid degradation under anaerobic conditions. The registered EPR spectra under irradiation that present in Figure 20 showed that all the photocatalysts (bare and modified) exhibited the same spectra, however, the intensities of the signals were different. In this study, it was found that the higher amount of photocatalyzed H_2 formed by employing Pt-TiO_2 as a photocatalyst, which become in agreement with the presented results in Figure 20 as the sample that contains the Pt-TiO_2 (Figure 20c) exhibit the stronger signal.

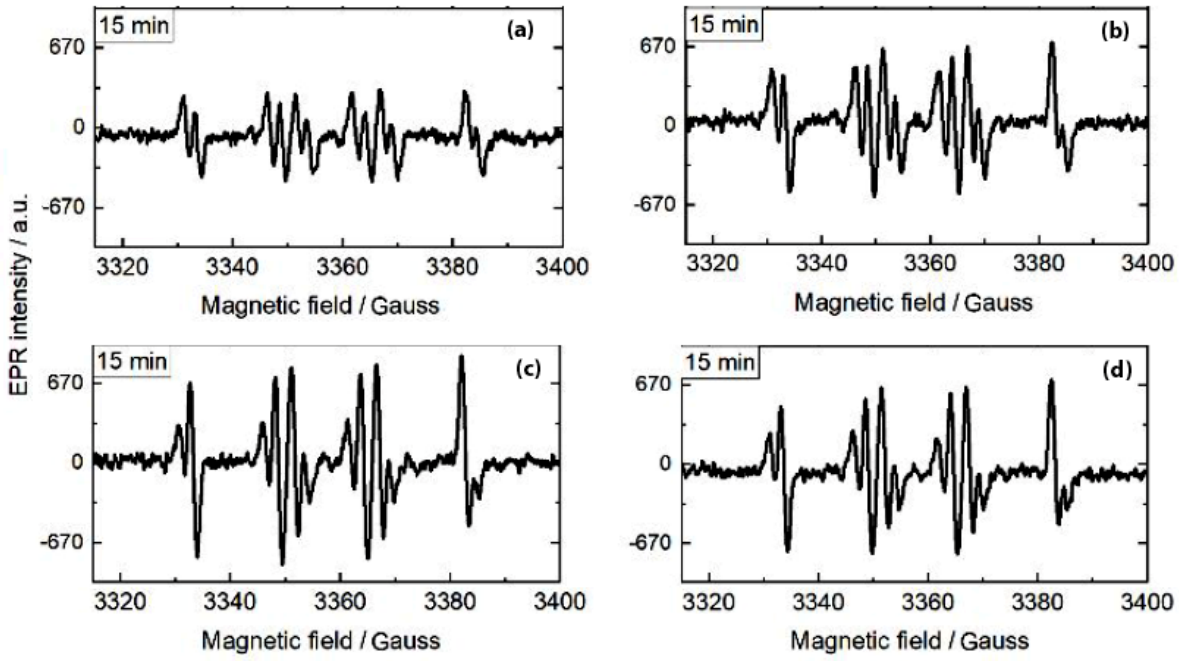

Figure 20. EPR spectra of aqueous suspensions of oxalic acid (5.5 mmol L^{-1} at pH ≈ 3)/DMPO (0.8 mmol L^{-1}) under UV irradiation in the presence of (1 g L^{-1}) bare TiO_2 (**a**) Au/TiO_2 (**b**) Pt/TiO_2 (**c**) and Au–Pt/TiO_2 (**d**) in O_2 free system. Adapted with permission from [21]. Copyright 2020 American Chemical Society.

Moreover, the authors suggested that the complex EPR signal (Figure 20) was formed due to the overlapping of different DMPO spin adducts produced during the photoreforming of oxalic acid. By simulating this spectrum (Figure 21), they claimed that DMPO•–CHO, DMPO•–(CO–CO_2^-), and DMPO•–CO_2^- were formed during this process. Although the authors did not observe the formation of •OH, however, they could not exclude their contribution in the photocatalytic process. However, the authors in another publication [97] performed EPR spin-trap experiments as described before but with the presence of KI as a

second hole scavenger in the addition to oxalic acid. They noticed that DMPO$^{\bullet}$-CO_2-spin adduct is the lonely signal detected in the presence of KI with much lower EPR intensities as presented in Figure 22. They explained this result by suggesting different pathways including the inhibition of by-products formation and lower $^{\bullet}CO_2^-$ radicals' production when KI was added to the suspension.

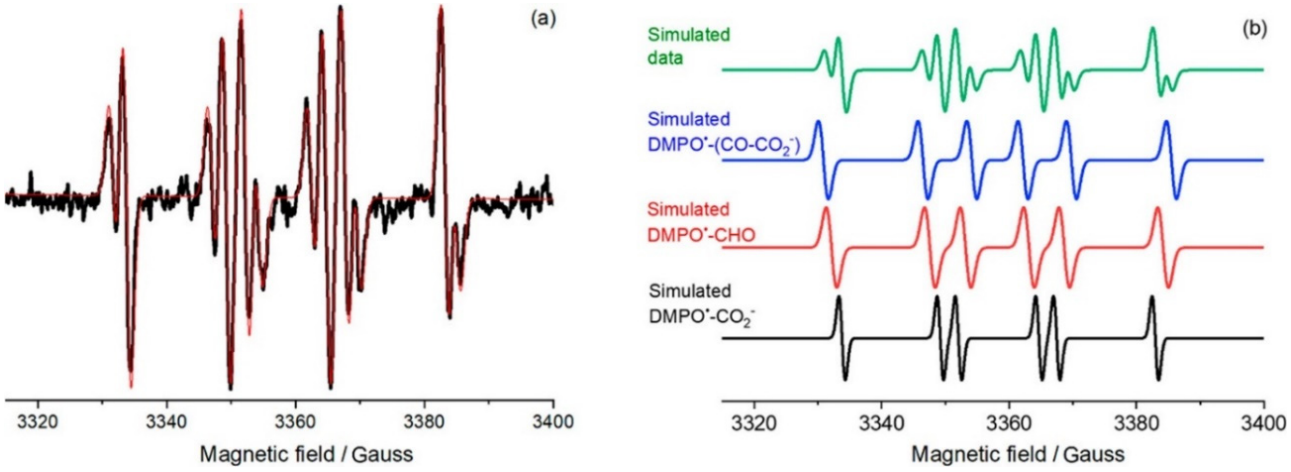

Figure 21. EPR spin-trap experiment in the absence of O_2 for a UV-irradiated oxalic acid suspension; (**a**) experimental spectrum (black) with its simulation (red) and (**b**) simulated spectrum of the mixed radicals and of each DMPO$^{\bullet}$-radical spin adduct. Adapted with permission from [21]. Copyright 2020 American Chemical Society.

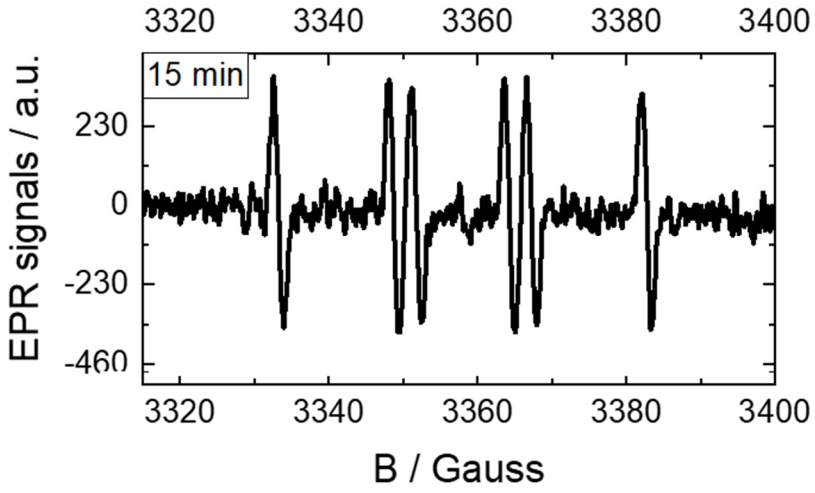

Figure 22. EPR spin trap spectrum in N_2 atmosphere for a UV-irradiated suspension contained oxalic acid (5.5 mmol L^{-1}), 20 mmol L^{-1} KI, DMPO (0.8 mmol L^{-1}), and Pt/TiO_2 (1 g L^{-1}). Adapted with permission from [97].

Although the TiO_2 has a thermodynamically feasible band structure for the water splitting (for both proton reduction and water oxidation under UV light irradiation) to H_2 and O_2, vast studies of the photocatalytic water splitting at TiO_2-based nanomaterials have shown that H_2 but not O_2 evolved during the photocatalytic process. To explain this phenomenon, Li et al., [98] studied the photocatalytic overall water splitting over three different phases of TiO_2, namely, anatase, rutile, and brookite. The authors found that the overall water splitting can only take place on rutile, while, it becomes feasible on anatase and brookite under prolonged UV irradiation. To explain these results, the authors employed the EPR spin-trap technique using DMPO as a spin trapping agent to probe the reactive oxygen species derived on the surface of different phases of TiO_2 under UV light

irradiation and Ar atmosphere. Under dark, no signal was detected for all photocatalysts, while, they obtained different signals for the three TiO_2 phases under light irradiation. Both anatase and brookite showed the same EPR signal consisting of four characteristic peaks with standard ratios of intensities 1:2:2:1, ascribed to $^{\bullet}$DMPO-OH adduct. On the other hand, the seven-line EPR signal that was detected for rutile TiO_2 ascribed to $^{\bullet}$DMPO-X generated from the oxidation of DMPO by peroxide, which can be easily decomposed to produce O_2 on rutile as the authors speculated. In the case of anatase and brookite TiO_2, the formed $^{\bullet}$OH radical may be strongly absorbed on the surface and its amount increases with the prolonged UV irradiation. Thus, at saturation of absorption, the coupling of the formed $^{\bullet}$OH radicals leads to evolving O_2 on the surface of the TiO_2.

Moreover, the spin trapping technique was not only used to detect and monitor the formed reactive species such as the oxygen and nitrogen reactive radicals [94,99] during the photocatalytic degradation process, but also is employed within the mechanistic pathway to monitor and/or to be involved in controlling the experimental conditions during the photocatalysis organic synthesis [82,100–102]. The involvement of TEMPO derivative radical within a mechanistic pathway of the synthesis reaction is assumed to act as a selective redox mediator involved in reactions of the generated reactive oxygen species. Balayeva et al. [101] studied the visible-light-induced dehydrogenation of N-heterocycles such as tetra-hydroquinolines, tetrahydroisoquinolines, and indolines compounds on the surface of TiO_2 in an aerated system yielding the corresponding heteroarenes compounds. In this study, the authors found that 4-amino-TEMPO exhibits a beneficial role, as it improved the yield and increased the selectivity of the dehydrogenation reaction. According to the authors, the low conversion and selectivity in the absence of 4-amino-TEMPO were attributed to the formation of H_2O_2/TiO_2 surface complexes (Equation (32)), thus, preventing the formation of the N-heterocycle$-TiO_2$ surface complex, which is necessary for the efficient electron transfer from the excited organic moiety to the TiO_2 conduction band. However, in presence of the TEMPO (paramagnetic), it will be oxidized to $TEMPO^+$ (not paramagnetic) and reduces the O_2 to $O_2^{-\bullet}$, Equation (33). The formed cation further reacts with H_2O_2/TiO_2 surface complex generated superoxide radical $O_2^{-\bullet}$, Equations (34) and (35). To confirm their hypothesis, the authors employed the EPR technique in this reaction to monitor the 4-amino-TEMPO signal under visible light illumination in this system. They found that the 4-amino-TEMPO signal slightly decreases upon illumination, which suggests that the cation 4-amino-$TEMPO^+$ is formed upon visible-light illumination.

$$H_2O_2 + Ti^{IV}_{(surf.)} \quad \leftrightarrow \quad Ti^{IV} - OOH_{(surf.)} + H^+ \tag{32}$$

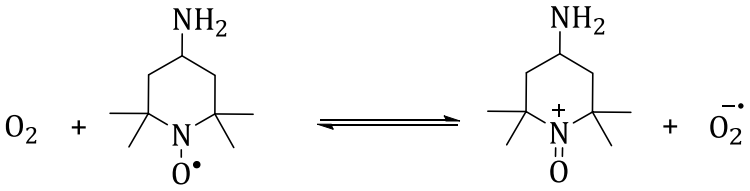

(33)

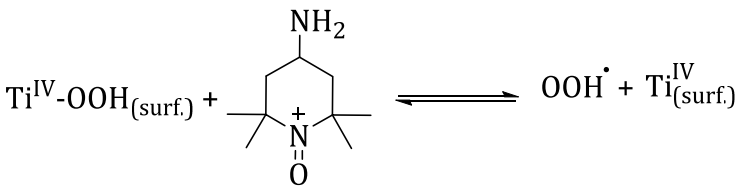

(34)

$$OOH^{\bullet} \rightleftharpoons O_2^{\bullet -} + H^+ \tag{35}$$

Furthermore, it is highly important to highlight that the fate of the photocatalytic reaction depends on the experimental conditions. In this regard, Mazzanti et al. [102]

demonstrated that the photocatalytic reaction of the azo dyes (methyl orange and acid orange 7) on the surface of the TiO_2 can be switched from the degradation path to the reductive path by introducing the sodium formate in the system. This change in the reaction conditions leads to the transformation of the azo dyes into useful products. In the absence of the sodium formate, the photocatalytic degradation of the azo dyes via the photogenerated hydroxyl radical leading to the formation of several independent pieces as secondary pollutants. The formation of the $^{\bullet}OH$ radical in this system was confirmed by photoexcitation of deaerated azo dye/TiO_2 suspensions in the presence of the spin trapping agent DMPO, which leads to the formation of a quartet EPR signal ascribable to the formation of $^{\bullet}$DMPO-OH adduct (Figure 23).

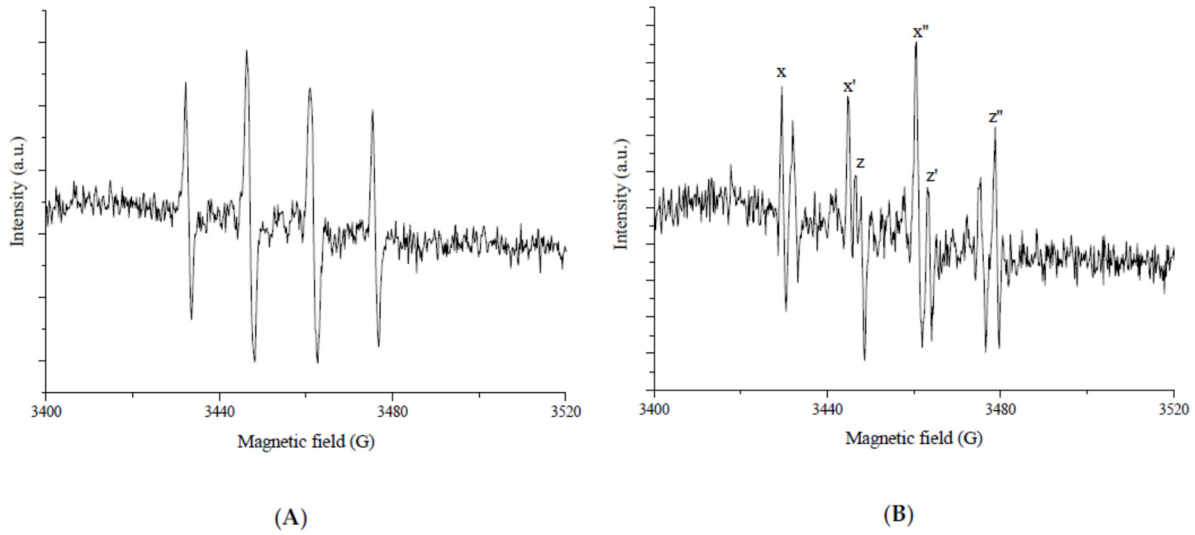

Figure 23. EPR spin trapping spectra obtained upon photoexcitation of the deaerated azo dye/TiO_2 suspensions containing the spin trap DMPO (**A**) and sodium formate (**B**).

However, the presence of the formate ion anion in the system leads to scavenge the photogenerated holes, thereby inhibiting the hydroxyl radical formation. Therefore, protons derived from the oxidation of formate by the photogenerated valance band holes and promoted electrons in the TiO_2 conduction band lead to the reductive cleavage of N=N bonds yielding reduced valuable intermediates such as sulfanilic acid. The EPR signal that formed in this system in the presence of formate ions showed a triplet of doublets signal ($^{\bullet}$DMPO-CO_2) attributed to the formation of $CO_2^{-\bullet}$ from oxidation of formate ions.

Some interesting mechanism studies were also performed in the literature using EPR measurements of Nb_2O_5 in suspension. Jiao and coworkers recently published a noteworthy case where simulated natural environment conditions were applied for photocatalytic studies [103]. They investigate some materials such as plastic bags, containers, and wrap films for food, and some of their components to be photoconverted by Nb_2O_5 without any sacrificial agents. The oxide was prepared in a way to obtain Nb_2O_5 layers composed of a single-unit-cell thickness, in order to maximize the available surface. The photoreaction was found to produce CO_2 which was further selectively photoreduced to CH_3COOH. By in situ EPR analysis, the oxide suspension evidenced the formation of DMPO-$OH^{\bullet}$ and DMPO-$O_2^{\bullet-}$ using pure water and methanol as the solvent, respectively. This result indicated that Nb_2O_5 photoexcited holes could oxidize H_2O into $^{\bullet}OH$ radicals and meanwhile the photogenerated electrons could reduce O_2 into $O_2^{\bullet-}$, H_2O_2 and H_2O. Along with further studies and other techniques, the mechanism was based on the oxidative C–C bond cleavage by O_2 and $^{\bullet}OH$ radical to form CO_2 which formed in sequence CH_3COOH by reductive photoinduced C–C coupling of $^{\bullet}COOH$ intermediates.

The same radicals have been reported in the work of Chen and coworkers [104]. The authors have prepared Nb_2O_5 nanospheres by the hydrothermal method which were

identified with the orthorhombic phase. The samples showed good photoactivity for Rhodamine B degradation under visible light. When EPR analysis was performed using a dispersion with Nb_2O_5 (Figure 24), DMPO, and the dye under visible light irradiation, the generation of $^{\bullet}OH$ was observed in water suspension whereas $O_2^{\bullet-}$ radicals were found in the presence of methanol. The higher intensity for the latter one could indicate that it would be the main active radical for the photodegradation of Rhodamine B. This fact was confirmed by photoluminescence experiments using different scavengers. Finally, the mechanism was explained based on a photosensitization for the photocatalytic oxidation and degradation of the dye on Nb_2O_5 under visible light.

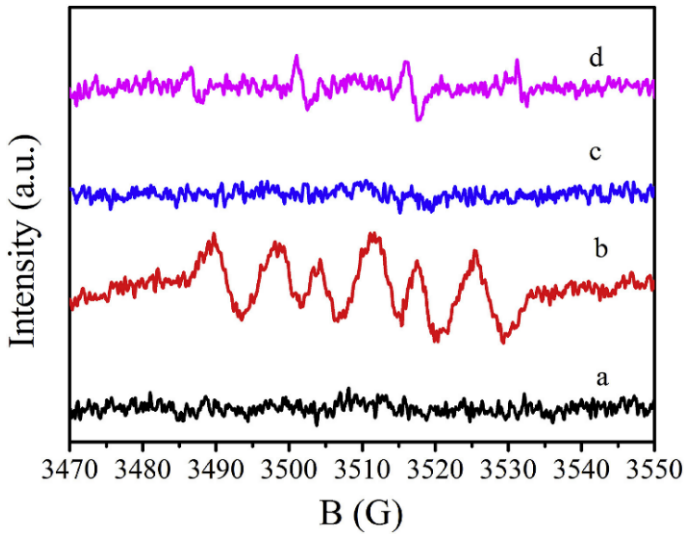

Figure 24. EPR spectra of the samples with DMPO spin-trapping (**a**,**b**) in methanol suspensions, and (**c**,**d**) in water suspensions: (**a**,**c**) under dark condition and (**b**,**d**) under visible light irradiation for 120 s. Reprinted with permission from [104].

Niobium oxide is also well known for H_2 evolution application and in many cases; deposited platinum is applied as a co-catalyst. In this sense, Zhang and coworkers have shown the performance of mesoporous Pt–Nb_2O_5 photocatalysts evaluating two different procedures, a sol-gel one-step method and by impregnation [105]. The materials were applied to H_2 generation in a methanolic solution under UV irradiation in which the sample prepared by one-step method resulted in a higher rate (9.79 mmol h^{-1}). The photocatalytic activity mechanism, in relation to the generated radicals and their whole reaction, was deeply investigated by EPR studies. In principle, the same kinds of radicals mentioned before were found also in this case. In presence of methanol, both $O_2^{\bullet-}$ and $CH_2OH^{\bullet}$ were detected for the tested samples under irradiation. Their intensities were higher for the one-step prepared sample, followed by the one produced by impregnation and then, the bare Nb_2O_5. When the analysis was run in water, $^{\bullet}OH$ radicals were identified with intensities following the same trend as for the other radicals. According to these results, it was possible to conclude that the efficiency of photogenerated charge carriers transfer from the photocatalyst has been enhanced by Pt nanoparticles, especially when applying the one-step method.

5. Conclusions

Tackling global warming and future fuel is one of the key challenges in the recent century. Amongst all the techniques to be used photocatalytic-based processes have the unique advantages that they solely utilize the most abundant solar energy without increasing greenhouse gases emissions. However, engineering a highly active photocatalytic material that fulfills all the industrial requirement strongly rely on a deep understanding of the fate of the photogenerated charge carriers upon irradiation of this material. Being amongst the

most suitable materials from the industrial point of view, TiO_2 and more recently Nb_2O_5 have been the focus of many researchers worldwide. EPR is a powerful technique that is practically beneficial in understanding the chemistry that occurs on the surface of metal oxide photocatalysis due to the low frequency of the electromagnetic radiation used for the spin resonance of electrons. This advantage assures no interference from the frequency of the light, allowing measuring the EPR spectra under irradiation in addition to the measurement in dark conditions. By means of the EPR technique, researchers are able to understand the effect of different factors on the intensity of the photogenerated electron-hole pairs in the bulk, at the surface, or on the trapping centers. This in turn influences the probability of electron transfer reactions and thus the overall process efficiency. These factors include the crystallinity and available phases of the material, the particle size, the presence of trapping centers and vacancies, loading with co-catalysts, as well as the surrounding media. As we have seen from the herein presented examples, a substantial research effort is needed to improve both the fundamental understanding of the numerous physicochemical effects involved in the photocatalytic processes and the means of translating these effects into practical outcomes. This makes the metal oxide-based photocatalysis field both exciting and challenging, especially for multidisciplinary collaborations.

Author Contributions: Conceptualization, methodology, investigation, O.A.-M., Y.A. and B.N.N. writing—original draft preparation, O.A.-M., Y.A., B.N.N. and M.C.; writing—review and editing, O.A.-M., Y.A., A.H., M.C. and A.O.T.P.; supervision, D.W.B. All authors have read and agreed to the published version of the manuscript.

Funding: Financial support from the Katholischer Akademischer Ausländer-Dienst (KAAD) and Graduiertenakademie at Gottfried Wilhelm Leibniz Universität Hannover are gratefully acknowledged for providing scholarships for Osama Al-Madanat to perform his PhD. B.N.N. gratefully acknowledges the financial support from CAPES, Brazil, from the CAPES/DAAD/CNPQ (15/2017) program, grant number 88887.161403/2017-00. M.C. acknowledges the funding from the European Union's Horizon 2020 research and innovation programme under the Marie Skłodowska-Curie grant agreement No 801474 and from the State Research Agency/Spanish Ministry of Science and Innovation (AEI/MICINN) through the Severo Ochoa Excellence Accreditation CEX2019-000925-S. The studies performed in the laboratory "Photoactive nanocomposite materials" were supported by Saint-Petersburg State University (ID: 73032813).

Data Availability Statement: This review did not report new data. The data presented here are available in the literature.

Conflicts of Interest: The authors declare no conflict of interest.

References

1. Schneider, J.; Matsuoka, M.; Takeuchi, M.; Zhang, J.; Horiuchi, Y.; Anpo, M.; Bahnemann, D.W. Understanding TiO_2 photocatalysis: Mechanisms and materials. *Chem. Rev.* **2014**, *114*, 9919–9986. [CrossRef]
2. Ramadan, W.; Zaki, M.I.; Fouad, N.E.; Mekhemer, G.A.H. Particle characteristics and reduction behavior of synthetic magnetite. *J. Magn. Magn. Mater.* **2014**, *355*, 246–253. [CrossRef]
3. Al-Madanat, O.; AlSalka, Y.; Ramadan, W.; Bahnemann, D.W. TiO_2 photocatalysis for the transformation of aromatic water pollutants into fuels. *Catalysts* **2021**, *11*, 317. [CrossRef]
4. Al-Madanat, O. Photocatalytic Transformation of Water Pollutants into Fuels. Ph.D. Thesis, Gottfried Wilhelm Leibniz Universität, Hannover, Germany, 2021.
5. AlSalka, Y. Photocatalytic Water Splitting for Solar Hydrogen Production and Simultaneous Decontamination of Organic Pollutants. Ph.D. Thesis, Gottfried Wilhelm Leibniz Universität, Hannover, Germany, 2020.
6. Takanabe, K. Photocatalytic water splitting: Quantitative approaches toward photocatalyst by design. *ACS Catal.* **2017**, *7*, 8006–8022. [CrossRef]
7. AlSalka, Y.; Granone, L.I.; Ramadan, W.; Hakki, A.; Dillert, R.; Bahnemann, D.W. Iron-based photocatalytic and photoelectrocatalytic nano-structures: Facts, perspectives, and expectations. *Appl. Catal. B Environ.* **2019**, *244*, 1065–1095. [CrossRef]
8. Weil, J.A.; Bolton, J.R. *Electron Paramagnetic Resonance*; John Wiley & Sons, Inc.: Hoboken, NJ, USA, 2006. [CrossRef]
9. Brustolon, M.; Giamello, E. *Electron Paramagnetic Resonance: A Practitioner's Toolkit*; John Wiley & Sons, Inc.: Hoboken, NJ, USA, 2009. [CrossRef]
10. Wang, Z.; Ma, W.; Chen, C.; Ji, H.; Zhao, J. Probing paramagnetic species in titania-based heterogeneous photocatalysis by electron spin resonance (ESR) spectroscopy—A mini review. *Chem. Eng. J.* **2011**, *170*, 353–362. [CrossRef]

11. Fittipaldi, M.; Gatteschi, D.; Fornasiero, P. The power of EPR techniques in revealing active sites in heterogeneous photocatalysis: The case of anion doped TiO_2. *Catal. Today* **2013**, *206*, 2–11. [CrossRef]
12. Chiesa, M.; Giamello, E.; Livraghi, S.; Paganini, M.C.; Polliotto, V.; Salvadori, E. Electron magnetic resonance in heterogeneous photocatalysis research. *J. Phys. Condens. Matter* **2019**, *31*, 444001. [CrossRef]
13. Qian, R.; Zong, H.; Schneider, J.; Zhou, G.; Zhao, T.; Li, Y.; Yang, J.; Bahnemann, D.W.; Pan, J.H. Charge carrier trapping, recombination and transfer during TiO_2 photocatalysis: An overview. *Catal. Today* **2019**, *335*, 78–90. [CrossRef]
14. Bahnemann, D.W.; Hilgendorff, M.; Memming, R. Charge carrier dynamics at TiO_2 particles: Reactivity of free and trapped holes. *J. Phys. Chem. B* **1997**, *101*, 4265–4275. [CrossRef]
15. Hoffmann, M.R.; Martin, S.T.; Choi, W.; Bahnemann, D.W. Environmental applications of semiconductor photocatalysis. *Chem. Rev.* **1995**, *95*, 69–96. [CrossRef]
16. Ahmed, A.Y.; Kandiel, T.A.; Ivanova, I.; Bahnemann, D. Photocatalytic and photoelectrochemical oxidation mechanisms of methanol on TiO_2 in aqueous solution. *Appl. Surf. Sci.* **2014**, *319*, 44–49. [CrossRef]
17. AlSalka, Y.; Hakki, A.; Fleisch, M.; Bahnemann, D.W. Understanding the degradation pathways of oxalic acid in different photocatalytic systems: Towards simultaneous photocatalytic hydrogen evolution. *J. Photochem. Photobiol. A Chem.* **2018**, *366*, 81–90. [CrossRef]
18. Salvador, P. On the nature of photogenerated radical species active in the oxidative degradation of dissolved pollutants with TiO_2 aqueous suspensions: A revision in the light of the electronic structure of adsorbed water. *J. Phys. Chem. C* **2007**, *111*, 17038–17043. [CrossRef]
19. Grela, M.A.; Coronel, M.E.J.; Colussi, A.J. Quantitative spin-trapping studies of weakly illuminated titanium dioxide Sols. Implications for the mechanism of photocatalysis. *J. Phys. Chem.* **1996**, *100*, 16940–16946. [CrossRef]
20. Perissinotti, L.L.; Brusa, M.A.; Grela, M.A. Yield of carboxyl anion radicals in the photocatalytic degradation of formate over TiO_2 particles. *Langmuir* **2001**, *17*, 8422–8427. [CrossRef]
21. AlSalka, Y.; Al-Madanat, O.; Curti, M.; Hakki, A.; Bahnemann, D.W. Photocatalytic H_2 evolution from oxalic acid: Effect of Co-catalysts and carbon dioxide radical anion on the surface charge transfer mechanisms. *ACS Appl. Energy Mater.* **2020**, *3*, 6678–6691. [CrossRef]
22. Dodd, N.J.F.; Jha, A.N. Photoexcitation of aqueous suspensions of titanium dioxide nanoparticles: An electron spin resonance spin trapping study of potentially oxidative reactions. *Photochem. Photobiol.* **2011**, *87*, 632–640. [CrossRef]
23. Gu, Q.; Long, J.; Fan, L.; Chen, L.; Zhao, L.; Lin, H.; Wang, X. Single-site Sn-grafted Ru/TiO_2 photocatalysts for biomass reforming: Synergistic effect of dual co-catalysts and molecular mechanism. *J. Catal.* **2013**, *303*, 141–155. [CrossRef]
24. Buettner, G.R.; Mason, R.P. 9 Spin-trapping methods for detecting superoxide and hydroxyl free radicals in vitro and in vivo. In *Methods in Enzymology*; Academic Press: New York, NY, USA, 1990; Volume 186, pp. 127–133.
25. Howe, R.F.; Gratzel, M. EPR observation of trapped electrons in colloidal titanium dioxide. *J. Phys. Chem.* **1985**, *89*, 4495–4499. [CrossRef]
26. Iorio, Y.D.; Aguirre, M.E.; Brusa, M.A.; Grela, M.A. Surface chemistry determines electron storage capabilities in alcoholic sols of titanium dioxide nanoparticles. A combined FTIR and room temperature EPR investigation. *J. Phys. Chem. C* **2012**, *116*, 9646–9652. [CrossRef]
27. Günnemann, C.; Curti, M.; Schneider, J.; Bahnemann, D.W. Dynamics of photoinduced bulk and surface reactions involving semiconductors characterized by time resolved spectroscopy techniques (2015–2018). *Photochemistry* **2020**, *47*, 122–158. [CrossRef]
28. Ramadan, W.; Kareem, M.; Hannoyer, B.; Saha, S. Effect of PH on the structural and magnetic properties of magnetite nanoparticles synthesised by co-precipitation. *Adv. Mater. Res.* **2011**, *324*, 129–132. [CrossRef]
29. Szczepankiewicz, S.H.; Moss, J.A.; Hoffmann, M.R. Electron traps and the stark effect on hydroxylated titania photocatalysts. *J. Phys. Chem. B* **2002**, *106*, 7654–7658. [CrossRef]
30. Szczepankiewicz, S.H.; Moss, J.A.; Hoffmann, M.R. Slow surface charge trapping kinetics on irradiated TiO_2. *J. Phys. Chem. B* **2002**, *106*, 2922–2927. [CrossRef]
31. Yoshihara, T.; Katoh, R.; Furube, A.; Tamaki, Y.; Murai, M.; Hara, K.; Murata, S.; Arakawa, H.; Tachiya, M. Identification of reactive species in photoexcited nanocrystalline TiO_2 films by wide-wavelength-range (400−2500 nm) transient absorption spectroscopy. *J. Phys. Chem. B* **2004**, *108*, 3817–3823. [CrossRef]
32. Katoh, R.; Furube, A.; Yamanaka, K.-I.; Morikawa, T. Charge separation and trapping in N-Doped TiO_2 photocatalysts: A time-resolved microwave conductivity study. *J. Phys. Chem. Lett.* **2010**, *1*, 3261–3265. [CrossRef]
33. Kolen'ko, Y.V.; Churagulov, B.R.; Kunst, M.; Mazerolles, L.; Colbeau-Justin, C. Photocatalytic properties of titania powders prepared by hydrothermal method. *Appl. Catal. B Environ.* **2004**, *54*, 51–58. [CrossRef]
34. Meichtry, J.M.; Colbeau-Justin, C.; Custo, G.; Litter, M.I. Preservation of the photocatalytic activity of TiO_2 by EDTA in the reductive transformation of Cr(VI). Studies by time resolved microwave conductivity. *Catal. Today* **2014**, *224*, 236–243. [CrossRef]
35. Berger, T.; Sterrer, M.; Diwald, O.; Knözinger, E.; Panayotov, D.; Thompson, T.L.; Yates, J.T. Light-Induced charge separation in anatase TiO_2 particles. *J. Phys. Chem. B* **2005**, *109*, 6061–6068. [CrossRef] [PubMed]
36. Liu, W.K.; Whitaker, K.M.; Smith, A.L.; Kittilstved, K.R.; Robinson, B.H.; Gamelin, D.R. Room-temperature electron spin dynamics in free-standing ZnO quantum dots. *Phys. Rev. Lett.* **2007**, *98*, 186804. [CrossRef] [PubMed]
37. Whitaker, K.M.; Ochsenbein, S.T.; Polinger, V.Z.; Gamelin, D.R. Electron confinement effects in the EPR spectra of colloidal n-Type ZnO quantum dots. *J. Phys. Chem. C* **2008**, *112*, 14331–14335. [CrossRef]

38. Hurum, D.C.; Agrios, A.G.; Gray, K.A.; Rajh, T.; Thurnauer, M.C. Explaining the enhanced photocatalytic activity of Degussa P25 mixed-phase TiO_2 using EPR. *J. Phys. Chem. B* **2003**, *107*, 4545–4549. [CrossRef]
39. Chiesa, M.; Paganini, M.C.; Livraghi, S.; Giamello, E. Charge trapping in TiO_2 polymorphs as seen by Electron Paramagnetic Resonance spectroscopy. *Phys. Chem. Chem. Phys.* **2013**, *15*, 9435–9447. [CrossRef]
40. Dimitrijevic, N.M.; Saponjic, Z.V.; Rabatic, B.M.; Poluektov, O.G.; Rajh, T. Effect of size and shape of nanocrystalline TiO_2 on photogenerated charges. An EPR study. *J. Phys. Chem. C* **2007**, *111*, 14597–14601. [CrossRef]
41. Livraghi, S.; Maurelli, S.; Paganini, M.C.; Chiesa, M.; Giamello, E. Probing the local environment of Ti^{3+} ions in TiO_2 (rutile) by ^{17}O HYSCORE. *Angew. Chem. Int. Ed.* **2011**, *50*, 8038–8040. [CrossRef]
42. Livraghi, S.; Chiesa, M.; Paganini, M.C.; Giamello, E. On the nature of reduced states in titanium dioxide as monitored by electron paramagnetic resonance. I: The anatase case. *J. Phys. Chem. C* **2011**, *115*, 25413–25421. [CrossRef]
43. Livraghi, S.; Rolando, M.; Maurelli, S.; Chiesa, M.; Paganini, M.C.; Giamello, E. Nature of of reduced states in titanium dioxide as monitored by electron paramagnetic resonance. II: Rutile and brookite cases. *J. Phys. Chem. C* **2014**, *118*, 22141–22148. [CrossRef]
44. AlSalka, Y.; Hakki, A.; Schneider, J.; Bahnemann, D.W. Co-catalyst-free photocatalytic hydrogen evolution on TiO_2: Synthesis of optimized photocatalyst through statistical material science. *Appl. Catal. B Environ.* **2018**, *238*, 422–433. [CrossRef]
45. Friehs, E.; AlSalka, Y.; Jonczyk, R.; Lavrentieva, A.; Jochums, A.; Walter, J.-G.; Stahl, F.; Scheper, T.; Bahnemann, D. Toxicity, phototoxicity and biocidal activity of nanoparticles employed in photocatalysis. *J. Photochem. Photobiol. C Photochem. Rev.* **2016**, *29*, 1–28. [CrossRef]
46. Chen, X.; Mao, S.S. Titanium dioxide nanomaterials: Synthesis, properties, modifications, and applications. *Chem. Rev.* **2007**, *107*, 2891–2959. [CrossRef] [PubMed]
47. Li, G.; Dimitrijevic, N.M.; Chen, L.; Nichols, J.M.; Rajh, T.; Gray, K.A. The important role of tetrahedral Ti^{4+} sites in the phase transformation and photocatalytic activity of TiO_2 nanocomposites. *J. Am. Chem. Soc.* **2008**, *130*, 5402–5403. [CrossRef]
48. Justicia, I.; Ordejón, P.; Canto, G.; Mozos, J.L.; Fraxedas, J.; Battiston, G.A.; Gerbasi, R.; Figueras, A. Designed self-Doped titanium oxide thin films for efficient visible-light photocatalysis. *Adv. Mater.* **2002**, *14*, 1399–1402. [CrossRef]
49. Henderson, M.A.; Epling, W.S.; Peden, C.H.F.; Perkins, C.L. Insights into photoexcited electron scavenging processes on TiO_2 obtained from studies of the reaction of O_2 with OH groups adsorbed at eectronic defects on TiO_2(110). *J. Phys. Chem. B* **2003**, *107*, 534–545. [CrossRef]
50. Mohamed, H.H.; Dillert, R.; Bahnemann, D.W. Reaction dynamics of the transfer of stored electrons on TiO_2 nanoparticles: A stopped flow study. *J. Photochem. Photobiol. A Chem.* **2011**, *217*, 271–274. [CrossRef]
51. Khomenko, V.M.; Langer, K.; Rager, H.; Fett, A. Electronic absorption by Ti^{3+} ions and electron delocalization in synthetic blue rutile. *Phys. Chem. Miner.* **1998**, *25*, 338–346. [CrossRef]
52. Kurtz, R.L.; Stock-Bauer, R.; Msdey, T.E.; Román, E.; De Segovia, J. Synchrotron radiation studies of H_2O adsorption on TiO_2(110). *Surf. Sci.* **1989**, *218*, 178–200. [CrossRef]
53. Chiesa, M.; Giamello, E.; Che, M. EPR characterization and reactivity of surface-localized inorganic radicals and radical ions. *Chem. Rev.* **2010**, *110*, 1320–1347. [CrossRef] [PubMed]
54. Morra, E.; Giamello, E.; Chiesa, M. EPR approaches to heterogeneous catalysis. The chemistry of titanium in heterogeneous catalysts and photocatalysts. *J. Magn. Reson.* **2017**, *280*, 89–102. [CrossRef] [PubMed]
55. Howe, R.F.; Gratzel, M. EPR study of hydrated anatase under UV irradiation. *J. Phys. Chem.* **1987**, *91*, 3906–3909. [CrossRef]
56. Micic, O.I.; Zhang, Y.; Cromack, K.R.; Trifunac, A.D.; Thurnauer, M.C. Trapped holes on titania colloids studied by electron paramagnetic resonance. *J. Phys. Chem.* **1993**, *97*, 7277–7283. [CrossRef]
57. Micic, O.; Zhang, Y.; Cromack, K.R.; Trifunac, A.; Thurnauer, M. Photoinduced hole transfer from titanium dioxide to methanol molecules in aqueous solution studied by electron paramagnetic resonance. *J. Phys. Chem.* **1993**, *97*, 13284–13288. [CrossRef]
58. Coronado, J.M.; Maira, A.J.; Conesa, J.C.; Yeung, K.L.; Augugliaro, V.; Soria, J. EPR study of the surface characteristics of nanostructured TiO_2 under UV irradiation. *Langmuir* **2001**, *17*, 5368–5374. [CrossRef]
59. Panarelli, E.G.; Livraghi, S.; Maurelli, S.; Polliotto, V.; Chiesa, M.; Giamello, E. Role of surface water molecules in stabilizing trapped hole centres in titanium dioxide (anatase) as monitored by electron paramagnetic resonance. *J. Photochem. Photobiol. A Chem.* **2016**, *322-323*, 27–34. [CrossRef]
60. Yan, Y.; Shi, W.; Peng, W.; Lin, Y.; Zhang, C.; Li, L.; Sun, Y.; Ju, H.; Zhu, J.; Ma, W.; et al. Proton-free electron-trapping feature of titanium dioxide nanoparticles without the characteristic blue color. *Commun. Chem.* **2019**, *2*, 88. [CrossRef]
61. Kumar, C.P.; Gopal, N.O.; Wang, T.C.; Wong, M.-S.; Ke, S.C. EPR investigation of TiO_2 nanoparticles with temperature-dependent properties. *J. Phys. Chem. B* **2006**, *110*, 5223–5229. [CrossRef]
62. Al-Madanat, O.; AlSalka, Y.; Dillert, R.; Bahnemann, D.W. Photocatalytic H_2 production from naphthalene by various TiO_2 photocatalysts: Impact of Pt loading and formation of intermediates. *Catalysts* **2021**, *11*, 107. [CrossRef]
63. Al-Madanat, O.; Curti, M.; Günnemann, C.; AlSalka, Y.; Dillert, R.; Bahnemann, D.W. TiO_2 photocatalysis: Impact of the platinum loading method on reductive and oxidative half-reactions. *Catal. Today* **2021**, *380*, 3–15. [CrossRef]
64. Nunes, B.N.; Faustino, L.A.; Muller, A.V.; Polo, A.S.; Patrocinio, A.O.T. Chapter 8-Nb_2O_5 dye-sensitized solar cells. In *Nanomaterials for Solar Cell Applications*; Thomas, S., Sakho, E.H.M., Kalarikkal, N., Oluwafemi, S.O., Wu, J., Eds.; Elsevier: Amsterdam, The Netherlands, 2019; pp. 287–322. [CrossRef]
65. Nunes, B.N.; Lopes, O.F.; Patrocinio, A.O.T.; Bahnemann, D.W. Recent advances in niobium-based materials for photocatalytic solar fuel production. *Catalysts* **2020**, *10*, 126. [CrossRef]

66. Soares, M.R.N.; Leite, S.; Nico, C.; Peres, M.; Fernandes, A.J.S.; Graça, M.P.F.; Matos, M.; Monteiro, R.; Monteiro, T.; Costa, F.M. Effect of processing method on physical properties of Nb_2O_5. *J. Eur. Ceram. Soc.* **2011**, *31*, 501–506. [CrossRef]
67. Su, K.; Liu, H.; Gao, Z.; Fornasiero, P.; Wang, F. Nb_2O_5-Based photocatalysts. *Adv. Sci.* **2021**, *8*, 2003156. [CrossRef] [PubMed]
68. Zhao, W.; Zhao, W.; Zhu, G.; Lin, T.; Xu, F.; Huang, F. Black Nb_2O_5 nanorods with improved solar absorption and enhanced photocatalytic activity. *Dalton Trans.* **2016**, *45*, 3888–3894. [CrossRef]
69. Su, K.; Liu, H.; Zeng, B.; Zhang, Z.; Luo, N.; Huang, Z.; Gao, Z.; Wang, F. Visible-light-driven selective oxidation of toluene into benzaldehyde over nitrogen-modified Nb_2O_5 nanomeshes. *ACS Catal.* **2020**, *10*, 1324–1333. [CrossRef]
70. Yan, J.; Wu, G.; Guan, N.; Li, L. Nb_2O_5/TiO_2 heterojunctions: Synthesis strategy and photocatalytic activity. *Appl. Catal. B Environ.* **2014**, *152–153*, 280–288. [CrossRef]
71. Shishido, T.; Miyatake, T.; Teramura, K.; Hitomi, Y.; Yamashita, H.; Tanaka, T. Mechanism of photooxidation of alcohol over Nb_2O_5. *J. Phys. Chem. C* **2009**, *113*, 18713–18718. [CrossRef]
72. Shishido, T.; Teramura, K.; Tanaka, T. A unique photo-activation mechanism by "in situ doping" for photo-assisted selective NO reduction with ammonia over TiO_2 and photooxidation of alcohols over Nb_2O_5. *Catal. Sci. Technol.* **2011**, *1*, 541–551. [CrossRef]
73. Furukawa, S.; Shishido, T.; Teramura, K.; Tanaka, T. Reaction mechanism of selective photooxidation of hydrocarbons over Nb_2O_5. *J. Phys. Chem. C* **2011**, *115*, 19320–19327. [CrossRef]
74. Tamai, K.; Murakami, K.; Hosokawa, S.; Asakura, H.; Teramura, K.; Tanaka, T. Visible-Light selective photooxidation of aromatic hydrocarbons via ligand-to-metal charge transfer transition on Nb_2O_5. *J. Phys. Chem. C* **2017**, *121*, 22854–22861. [CrossRef]
75. Furukawa, S.; Ohno, Y.; Shishido, T.; Teramura, K.; Tanaka, T. Reaction mechanism of selective photooxidation of amines over niobium oxide: Visible-light-induced electron transfer between adsorbed amine and Nb_2O_5. *J. Phys. Chem. C* **2013**, *117*, 442–450. [CrossRef]
76. Janzen, E.G.; Blackburn, B.J. Detection and identification of short-lived free radicals by electron spin resonance trapping techniques (spin trapping). Photolysis of organolead, -tin, and -mercury compounds. *J. Am. Chem. Soc.* **1969**, *91*, 4481–4490. [CrossRef]
77. Lagercrantz, C. Spin trapping of some short-lived radicals by the nitroxide method. *J. Phys. Chem.* **1971**, *75*, 3466–3475. [CrossRef]
78. Ouari, O.; Hardy, M.; Karoui, H.; Tordo, P. Recent developments and applications of the coupled EPR/Spin trapping technique (EPR/ST). In *Electron Paramagnetic Resonance: Volume 22*; The Royal Society of Chemistry: London, UK, 2011; Volume 22, pp. 1–40.
79. Villamena, F.A. Chapter 5-EPR spin trapping. In *Reactive Species Detection in Biology*; Villamena, F.A., Ed.; Elsevier: Boston, MA, USA, 2017; pp. 163–202. [CrossRef]
80. Rosen, G.M.; Finkelstein, E.; Rauckman, E.J. A method for the detection of superoxide in biological systems. *Arch. Biochem. Biophys.* **1982**, *215*, 367–378. [CrossRef]
81. Gimat, A.; Kasneryk, V.; Dupont, A.-L.; Paris, S.; Averseng, F.; Fournier, J.; Massiani, P.; Rouchon, V. Investigating the DMPO-formate spin trapping method for the study of paper iron gall ink corrosion. *New J. Chem.* **2016**, *40*, 9098–9110. [CrossRef]
82. Dvoranova, D.; Barbierikova, Z.; Brezova, V. Radical intermediates in photoinduced reactions on TiO_2 (an EPR spin trapping study). *Molecules* **2014**, *19*, 17279–17304. [CrossRef]
83. Bard, A.J.; Gilbert, J.C.; Goodin, R.D. Application of spin trapping to the detection of radical intermediates in electrochemical transformations. *J. Am. Chem. Soc.* **1974**, *96*, 620–621. [CrossRef]
84. Konaka, R.; Kawai, M.; Noda, H.; Kohno, M.; Niwa, R. Synthesis and evaluation of DMPO-Type spin traps. *Free. Radic. Res.* **1995**, *23*, 15–25. [CrossRef]
85. Buettner, G.R. Spin trapping: ESR parameters of spin adducts 1474 1528V. *Free. Radic. Biol. Med.* **1987**, *3*, 259–303. [CrossRef]
86. He, W.; Liu, Y.; Wamer, W.G.; Yin, J.-J. Electron spin resonance spectroscopy for the study of nanomaterial-mediated generation of reactive oxygen species. *J. Food Drug Anal.* **2014**, *22*, 49–63. [CrossRef] [PubMed]
87. Al-Madanat, O.; Alsalka, Y.; Curti, M.; Dillert, R.; Bahnemann, D.W. Mechanistic iInsights into hydrogen evolution by photocatalytic reforming of naphthalene. *ACS Catal.* **2020**, *10*, 7398–7412. [CrossRef]
88. Belhadj, H.; Melchers, S.; Robertson, P.K.J.; Bahnemann, D.W. Pathways of the photocatalytic reaction of acetate in H_2O and D_2O: A combined EPR and ATR-FTIR study. *J. Catal.* **2016**, *344*, 831–840. [CrossRef]
89. Clément, J.-L.; Ferré, N.; Siri, D.; Karoui, H.; Rockenbauer, A.; Tordo, P. Assignment of the EPR spectrum of 5,5-Dimethyl-1-pyrroline N-Oxide (DMPO) superoxide spin adduct. *J. Org. Chem.* **2005**, *70*, 1198–1203. [CrossRef] [PubMed]
90. Jaeger, C.D.; Bard, A.J. Spin trapping and electron spin resonance detection of radical intermediates in the photodecomposition of water at titanium dioxide particulate systems. *J. Phys. Chem.* **1979**, *83*, 3146–3152. [CrossRef]
91. Yin, J.-J.; Liu, J.; Ehrenshaft, M.; Roberts, J.E.; Fu, P.P.; Mason, R.P.; Zhao, B. Phototoxicity of nano titanium dioxides in HaCaT keratinocytes—Generation of reactive oxygen species and cell damage. *Toxicol. Appl. Pharmacol.* **2012**, *263*, 81–88. [CrossRef] [PubMed]
92. Fu, H.; Zhang, L.; Zhang, S.; Zhu, Y.; Zhao, J. Electron spin resonance spin-trapping detection of radical intermediates in N-Doped TiO_2-Assisted photodegradation of 4-Chlorophenol. *J. Phys. Chem. B* **2006**, *110*, 3061–3065. [CrossRef] [PubMed]
93. Molinari, A.; Samiolo, L.; Amadelli, R. EPR spin trapping evidence of radical intermediates in the photo-reduction of bicarbonate/CO_2 in TiO_2 aqueous suspensions. *Photochem. Photobiol. Sci.* **2015**, *14*, 1039–1046. [CrossRef] [PubMed]
94. Schneider, J.T.; Firak, D.S.; Ribeiro, R.R.; Peralta-Zamora, P. Use of scavenger agents in heterogeneous photocatalysis: Truths, half-truths, and misinterpretations. *Phys. Chem. Chem. Phys.* **2020**, *22*, 15723–15733. [CrossRef] [PubMed]
95. Brezová, V.; Dvoranová, D.; Staško, A. Characterization of titanium dioxide photoactivity following the formation of radicals by EPR spectroscopy. *Res. Chem. Intermed.* **2007**, *33*, 251–268. [CrossRef]

96. Stefan, M.; Leostean, C.; Toloman, D.; Popa, A.; Macavei, S.; Falamas, A.; Suciu, R.; Barbu-Tudoran, L.; Marincas, O.; Pana, O. New emerging magnetic, optical and photocatalytic properties of Tb doped TiO_2 interfaced with $CoFe_2O_4$ nanoparticles. *Appl. Surf. Sci.* **2021**, *570*, 151172. [CrossRef]
97. Alsalka, Y.; Al-Madanat, O.; Hakki, A.; Bahnemann, D.W. Boosting the H_2 production efficiency via photocatalytic organic reforming: The role of additional hole scavenging system. *Catalysts* **2021**, *11*, 1423. [CrossRef]
98. Li, R.; Weng, Y.; Zhou, X.; Wang, X.; Mi, Y.; Chong, R.; Han, H.; Li, C. Achieving overall water splitting using titanium dioxide-based photocatalysts of different phases. *Energy Environ. Sci.* **2015**, *8*, 2377–2382. [CrossRef]
99. Brezova, V.; Barbierikova, Z.; Dvoranova, D.; Stasko, A. UVA-Induced processes in the aqueous Titanium Dioxide suspensions containing nitrite (an EPR spin trapping study). *J. Adv. Oxid. Technol.* **2016**, *19*, 290–301. [CrossRef]
100. Speckmeier, E.; Zeitler, K. Chapter 3 Practical aspects of photocatalysis. In *Photocatalysis in Organic Synthesis*, 1st ed.; Georg Thieme Verlag: Stuttgart, Germany, 2019.
101. Balayeva, N.O.; Zheng, N.; Dillert, R.; Bahnemann, D.W. Visible-Light-Mediated photocatalytic aerobic dehydrogenation of N-heterocycles by surface-grafted TiO_2 and 4-amino-TEMPO. *ACS Catal.* **2019**, *9*, 10694–10704. [CrossRef]
102. Mazzanti, M.; Caramori, S.; Fogagnolo, M.; Cristino, V.; Molinari, A. Turning waste into useful products by photocatalysis with nanocrystalline TiO_2 thin films: Reductive cleavage of azo bond in the presence of aqueous formate. *Nanomaterials* **2020**, *10*, 2147. [CrossRef] [PubMed]
103. Jiao, X.; Zheng, K.; Chen, Q.; Li, X.; Li, Y.; Shao, W.; Xu, J.; Zhu, J.; Pan, Y.; Sun, Y.; et al. Photocatalytic conversion of waste plastics into C2 fuels under simulated natural environment conditions. *J. Ger. Chem. Soc.* **2020**, *59*, 15497–15501. [CrossRef]
104. Chen, J.; Wang, H.; Huang, G.; Zhang, Z.; Han, L.; Song, W.; Li, M.; Zhang, Y. Facile synthesis of urchin-like hierarchical Nb_2O_5 nanospheres with enhanced visible light photocatalytic activity. *J. Alloy. Compd.* **2017**, *728*, 19–28. [CrossRef]
105. Zhang, H.; Lin, Q.; Ning, S.; Zhou, Y.; Lin, H.; Long, J.; Zhang, Z.; Wang, X. One-step synthesis of mesoporous Pt–Nb_2O_5 nanocomposites with enhanced photocatalytic hydrogen production activity. *RSC Adv.* **2016**, *6*, 96809–96815. [CrossRef]